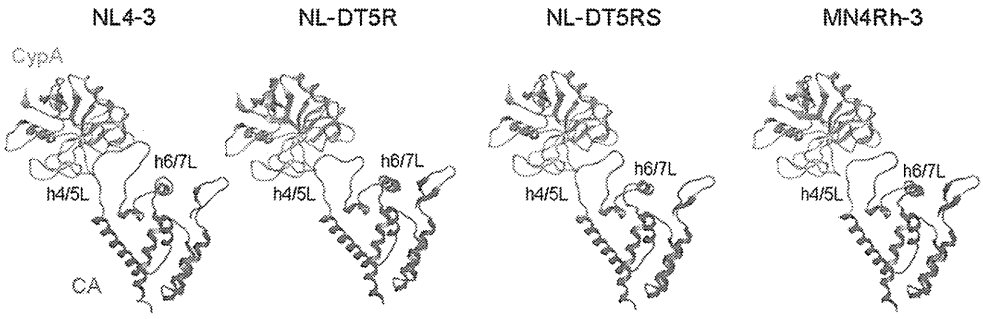

	NL4-3	NL-DT5R	NL-DT5RS	MN4Rh-3
CA	HIV-1 CA	h4/5L from SIVmac239	h4/5L and h6/7L from SIVmac239	h4/5L and h6/7L from SIVmac239 and Q110D
Binding energy (kcal/mol)	-64.447	-31.012	-36.071	-30.051

Fig. 6. Structural models of HIV CA NTD bound to CypA. The model of CA NTD bound to CypA was constructed by homology modeling using the crystal structure of HIV-1 CA NTD and CypA complex (PDB code: 1M9C [28]). The binding energies, E_{bind} (kcal/mol), of the complex were calculated using MOE as described previously [42,43]. The formula $E_{bind} = E_{complex} - (E_{CA} + E_{CypA})$ was used for the E_{bind} calculation, where $E_{complex}$ is the energy of the CA/CypA complex models, E_{CA} is the energy of the CA monomer model, and E_{CypA} is the energy of the CypA monomer model.

domain [46]. Thus, it is not unreasonable to assume that the replication of MN4Rh-3 carrying CA-Q110D is enhanced in macaque cells but reduced in human cells by augmenting its dissociation from CypA (Fig. 6). However, it was found to be difficult to experimentally confirm this structural insight by determining the effect of cyclosporine A or of siRNA against CypA on viral infectivity because interaction between the HIV-1mt CA and CypA was so weak. Alternatively, CA-Q110D may contribute to the alteration of the affinity to unknown anti-CA factor(s) other than CypA and TRIM5 proteins. In this case, it is speculated that the factor(s) might act negatively on HIV-1 replication in macaque cells but positively in human cells, and vice versa. Further study is required to elucidate the mechanism for enhancement of viral growth potential by CA-Q110D.

In conclusion, further modification of the HIV-1mt genome is necessary to overcome unconquered replication block(s) present in macaque cells and obtain viral clones similarly replication-competent in macaque cells and pathogenic for animals with SIVmac (Fig. 5). Considering the genome structure of MN4Rh-3 and the results presented here, major targets for modification now are *gag*-CA (against TRIM5α) and *vpu* (against tetherin). Gag-CA is one of the two principal viral determinants (CA and Vif) for the HIV-1 species-tropism. Construction of HIV-1 CA that evades from TRIM5α restriction is also useful for elucidation of the less-defined CA-TRIM5α interaction and antiviral mechanism of TRIM5α. Tetherin, identified as anti-virion release factor, is antagonized by Vpu [47,48], but macaque tetherin was not counteracted by HIV-1 Vpu [49]. Construction of HIV-1 Vpu that down-modulate macaque tetherin may enhance viral replication *in vivo* as well as *in vitro* [50]. Through these approaches, we may be able to precisely analyze HIV-1 replication and pathogenesis *in vivo* and provide new strategies against HIV-1/AIDS.

Acknowledgments

This study was supported by a grant from the Ministry of Health, Labor and Welfare of Japan (Research on HIV/AIDS project no. H23-003).

References

[1] M.H. Malim, M. Emerman, HIV-1 accessory proteins–ensuring viral survival in a hostile environment, Cell Host Microbe 3 (2008) 388–398.
[2] F. Kirchhoff, Immune evasion and counteraction of restriction factors by HIV-1 and other primate lentiviruses, Cell Host Microbe 8 (2010) 55–67.
[3] R. Shibata, H. Sakai, M. Kawamura, K. Tokunaga, A. Adachi, Early replication block of human immunodeficiency virus type 1 in monkey cells, J. Gen. Virol. 76 (1995) 2723–2730.
[4] M. Nomaguchi, N. Doi, K. Kamada, A. Adachi, Species barrier of HIV-1 and its jumping by virus engineering, Rev. Med. Virol. 18 (2008) 261–275.
[5] M. Nomaguchi, A. Adachi, Virology as biosystematics: towards understanding the viral infection biology, Front. Microbiol. 1 (2010) 2.
[6] R.K. Holmes, M.H. Malim, K.N. Bishop, APOBEC-mediated viral restriction: not simply editing? Trends Biochem. Sci. 32 (2007) 118–128.
[7] H. Huthoff, G.J. Towers, Restriction of retroviral replication by APOBEC3G/F and TRIM5alpha, Trends Microbiol. 16 (2008) 612–619.
[8] K. Strebel, J. Luban, K.T. Jeang, Human cellular restriction factors that target HIV-1 replication, BMC Med. 7 (2009) 48.
[9] J. Luban, Cyclophilin A, TRIM5, and resistance to human immunodeficiency virus type 1 infection, J. Virol. 81 (2007) 1054–1061.
[10] G.J. Towers, The control of viral infection by tripartite motif proteins and cyclophilin A, Retrovirology 4 (2007) 40.
[11] E.E. Nakayama, T. Shioda, Anti-retroviral activity of TRIM5 alpha, Rev. Med. Virol. 20 (2010) 77–92.
[12] R.M. Newman, L. Hall, M. Connole, G.L. Chen, S. Sato, E. Yuste, W. Diehl, E. Hunter, A. Kaur, G.M. Miller, W.E. Johnson, Balancing selection and the evolution of functional polymorphism in old world monkey TRIM5alpha, Proc. Natl. Acad. Sci. U. S. A. 103 (2006) 19134–19139.
[13] S.J. Wilson, B.L. Webb, L.M. Ylinen, E. Verschoor, J.L. Heeney, G.J. Towers, Independent evolution of an antiviral TRIMCyp in rhesus macaques, Proc. Natl. Acad. Sci. U. S. A. 105 (2008) 3557–3562.

[14] A.J. Price, F. Marzetta, M. Lammers, L.M. Ylinen, T. Schaller, S.J. Wilson, G.J. Towers, L.C. James, Active site remodeling switches HIV specificity of antiretroviral TRIMCyp, Nat. Struct. Mol. Biol. 16 (2009) 1036–1042.
[15] L.M. Ylinen, A.J. Price, J. Rasaiyaah, S. Hué, N.J. Rose, F. Marzetta, L.C. James, G.J. Towers, Conformational adaptation of Asian macaque TRIMCyp directs lineage specific antiviral activity, PLoS Pathog. 6 (2010) e1001062.
[16] K. Kamada, T. Igarashi, M.A. Martin, B. Khamsri, K. Hatcho, T. Yamashita, M. Fujita, T. Uchiyama, A. Adachi, Generation of HIV-1 derivatives that productively infect macaque monkey lymphoid cells, Proc. Natl. Acad. Sci. U. S. A. 103 (2006) 16959–16964.
[17] T. Igarashi, R. Iyengar, R.A. Byrum, A. Buckler-White, R.L. Dewar, C.E. Buckler, H.C. Lane, K. Kamada, A. Adachi, M.A. Martin, Human immunodeficiency virus type 1 derivative with 7% simian immunodeficiency virus genetic content is able to establish infections in pig-tailed macaques, J. Virol. 81 (2007) 11549–11552.
[18] K. Kamada, T. Yamashita, K. Hatcho, A. Adachi, M. Nomaguchi, Evasion from CypA- and APOBEC-mediated restrictions is insufficient for HIV-1 to efficiently grow in simian cells, Microbes Infect. 11 (2009) 164–171.
[19] A. Saito, M. Nomaguchi, S. Iijima, A. Kuroishi, T. Yoshida, Y.J. Lee, T. Hayakawa, K. Kono, E.E. Nakayama, T. Shioda, Y. Yasutomi, A. Adachi, T. Matano, H. Akari, Improved capacity of a monkey-tropic HIV-1 derivative to replicate in cynomolgus monkeys with minimal modifications, Microbes Infect. 13 (2011) 58–64.
[20] A. Kuroishi, A. Saito, Y. Shingai, T. Shioda, M. Nomaguchi, A. Adachi, H. Akari, E.E. Nakayama, Modification of a loop sequence between alpha-helices 6 and 7 of virus capsid (CA) protein in a human immunodeficiency virus type 1 (HIV-1) derivative that has simian immunodeficiency virus (SIVmac239) vif and CA alpha-helices 4 and 5 loop improves replication in cynomolgus monkey cells, Retrovirology 6 (2009) 70.
[21] T. Yamashita, N. Doi, A. Adachi, M. Nomaguchi, Growth ability in simian cells of monkey cell-tropic HIV-1 is greatly affected by downstream region of the vif gene, J. Med. Invest. 55 (2008) 236–240.
[22] M. Yamashita, M. Emerman, Capsid is a dominant determinant of retrovirus infectivity in nondividing cells, J. Virol. 78 (2004) 5670–5678.
[23] J.S. Lebkowski, S. Clancy, M.P. Calos, Simian virus 40 replication in adenovirus-transformed human cells antagonizes gene expression, Nature 317 (1985) 169–171.
[24] H. Akari, T. Fukumori, S. Iida, A. Adachi, Induction of apoptosis in herpesvirus saimiri-immortalized T lymphocytes by blocking interaction of CD28 with CD80/CD86, Biochem. Biophys. Res. Commun. 263 (1999) 352–356.
[25] N. Doi, S. Fujiwara, A. Adachi, M. Nomaguchi, Growth ability in various macaque cell lines of HIV-1 with simian cell-tropism, J. Med. Invest. 57 (2010) 284–292.
[26] A. Adachi, H.E. Gendelman, S. Koenig, T. Folks, R. Willey, A. Rabson, M.A. Martin, Production of acquired immunodeficiency syndrome-associated retrovirus in human and nonhuman cells transfected with an infectious molecular clone, J. Virol. 59 (1986) 284–291.
[27] U. O'Doherty, W.J. Swiggard, M.H. Malim, Human immunodeficiency virus type 1 spinoculation enhances infection through virus binding, J. Virol. 74 (2004) 10074–10080.
[28] B.R. Howard, F.F. Vajdos, S. Li, W.I. Sundquist, C.P. Hill, Structural insights into the catalytic mechanism of cyclophilin A, Nat. Struct. Biol. 10 (2003) 475–481.
[29] N. Deshpande, K.J. Addess, W.F. Bluhm, J.C. Merino-Ott, W. Townsend-Merino, Q. Zhang, C. Knezevich, L. Xie, L. Chen, Z. Feng, R.K. Green, J.L. Flippen-Anderson, J. Westbrook, H.M. Berman, P.E. Bourne, The RCSB protein data bank: a redesigned query system and relational database based on the mmCIF schema, Nucleic Acids Res. 33 (Database issue) (2005) D233–D237.
[30] H. Song, E.E. Nakayama, M. Yokoyama, H. Sato, J.A. Levy, T. Shioda, A single amino acid of the human immunodeficiency virus type 2 capsid affects its replication in the presence of cynomolgus monkey and human TRIM5alphas, J. Virol. 81 (2007) 7280–7285.
[31] K. Kono, H. Song, M. Yokoyama, H. Sato, T. Shioda, E.E. Nakayama, Multiple sites in the N-terminal half of simian immunodeficiency virus capsid protein contribute to evasion from rhesus monkey TRIM5α-mediated restriction, Retrovirology 7 (2010) 72.
[32] N. Inagaki, H. Takeuchi, M. Yokoyama, H. Sato, A. Ryo, H. Yamamoto, M. Kawada, T. Matano, A structural constraint for functional interaction between N-terminal and C-terminal domains in simian immunodeficiency virus capsid proteins, Retrovirology 7 (2010) 90.
[33] P. Labute, The generalized Born/volume integral implicit solvent model: estimation of the free energy of hydration using London dispersion instead of atomic surface area, J. Comput. Chem. 29 (2008) 1693–1698.
[34] J.W. Ponder, D.A. Case, Force fields for protein simulations, Adv. Protein Chem. 66 (2003) 27–85.
[35] A. Onufriev, D. Bashford, D.A. Case, Modification of the generalized Born model suitable for macromolecules, J. Phys. Chem. B 104 (2000) 3712–3720.
[36] T.Y. Lin, M. Emerman, Determinants of cyclophilin A-dependent TRIM5 alpha restriction against HIV-1, Virology 379 (2008) 335–341.
[37] A. Kuroishi, K. Bozek, T. Shioda, E.E. Nakayama, A single amino acid substitution of the human immunodeficiency virus type 1 capsid protein affects viral sensitivity to TRIM5 alpha, Retrovirology 7 (2010) 58.
[38] M. Stremlau, C.M. Owens, M.J. Perron, M. Kiessling, P. Autissier, J. Sodroski, The cytoplasmic body component TRIM5alpha restricts HIV-1 infection in old world monkeys, Nature 427 (2004) 848–853.
[39] Z. Keckesova, L.M. Ylinen, G.J. Towers, Cyclophilin A renders human immunodeficiency virus type 1 sensitive to old world monkey but not human TRIM5 alpha antiviral activity, J. Virol. 80 (2006) 4683–4690.
[40] E. Sokolskaja, L. Berthoux, J. Luban, Cyclophilin A and TRIM5alpha independently regulate human immunodeficiency virus type 1 infectivity in human cells, J. Virol. 80 (2006) 2855–2862.
[41] S.Y. Lim, T. Rogers, T. Chan, J.B. Whitney, J. Kim, J. Sodroski, N.L. Letvin, TRIM5alpha modulates immunodeficiency virus control in rhesus monkeys, PLoS Pathog. 6 (2010) e1000738.
[42] C.O. Onyango, A. Leligdowicz, M. Yokoyama, H. Sato, H. Song, E.E. Nakayama, T. Shioda, T. de Silva, J. Townend, A. Jaye, H. Whittle, S. Rowland-Jones, M. Cotten, HIV-2 capsids distinguish high and low virus load patients in a West African community cohort, Vaccine 28 (2010) B60–B67.
[43] M. Kinomoto, R. Appiah-Opong, J.A. Brandful, M. Yokoyama, N. Nii-Trebi, E. Ugly-Kwame, H. Sato, D. Ofori-Adjei, T. Kurata, F. Barre-Sinoussi, T. Sata, K. Tokunaga, HIV-1 proteases from drug-naive West African patients are differentially less susceptible to protease inhibitors, Clin. Infect. Dis. 41 (2005) 243–251.
[44] R.K. Gitti, B.M. Lee, J. Walker, M.F. Summers, S. Yoo, W.I. Sundquist, Structure of the amino-terminal core domain of the HIV-1 capsid protein, Science 273 (1996) 231–235.
[45] C. Tang, Y. Ndassa, M.F. Summers, Structure of the N-terminal 283-residue fragment of the immature HIV-1 Gag polyprotein, Nat. Struct. Biol. 9 (2002) 537–543.
[46] M. Yokoyama, S. Naganawa, K. Yoshimura, S. Matsushita, H. Sato, Structural dynamics of HIV-1 envelope Gp120 outer domain with V3 loop, PLoS One 7 (2012) e37530.
[47] S.J. Neil, T. Zang, P.D. Bieniasz, Tetherin inhibits retrovirus release and is antagonized by HIV-1 Vpu, Nature 451 (2008) 425–430.
[48] N. Van Damme, D. Goff, C. Katsura, R.L. Jorgenson, R. Mitchell, M.C. Johnson, E.B. Stephens, J. Guatelli, The interferon-induced protein BST-2 restricts HIV-1 release and is downregulated from the cell surface by the viral Vpu protein, Cell Host Microbe 3 (2008) 245–252.
[49] D. Sauter, M. Schindler, A. Specht, W.N. Landford, J. Münch, K.A. Kim, J. Votteler, U. Schubert, F. Bibollet-Ruche, B.F. Keele, J. Takehisa, Y. Ogando, C. Ochsenbauer, J.C. Kappes, A. Ayouba, M. Peeters, G.H. Learn, G. Shaw, P.M. Sharp, P. Bieniasz, B.H. Hahn, T. Hatziioannou, F. Kirchhoff, Tetherin-driven adaptation of Vpu and Nef function and the evolution of pandemic and nonpandemic HIV-1 strains, Cell Host Microbe 6 (2009) 409–421.
[50] M. Shingai, T. Yoshida, M.A. Martin, K. Strebel, Some human immunodeficiency virus type 1 Vpu proteins are able to antagonize macaque BST-2 in vitro and in vivo: Vpu-negative simian-human immunodeficiency viruses are attenuated in vivo, J. Virol. 85 (2011) 9708–9715.

frontiers in
MICROBIOLOGY

EDITORIAL
published: 08 August 2012
doi: 10.3389/fmicb.2012.00289

Receptor usage and the pathogenesis in acute and chronic virus infections

Yasuko Tsunetsugu-Yokota* and Kazutaka Terahara

Department of Immunology, National Institute of Infectious Diseases, Tokyo, Japan
**Correspondence: yyokota@nih.go.jp*

Edited by:
Akio Adachi, The University of Tokushima Graduate School, Japan

Reviewed by:
Akio Adachi, The University of Tokushima Graduate School, Japan

In the first phase of the viral life cycle, the virus enters cells using a specific cell surface receptor. Many viruses use multiple receptors: some of which are unique to a certain cell type, whereas others are found in many cell types. After the virus enters into cells, various cellular proteins may interact with it; some support virus replication, while others inhibit it. Once virus succeeds to establish its life cycle in the target cell, the progeny viruses disseminate within the tissues or systemically via viremia. The intrinsic pro- or anti-viral cellular machinery differs among cell types. Thus, depending on the receptors used, the viral cell tropism is determined, resulting in the characteristic distribution of virus-infected cells/tissues and the disease outcome *in vivo*.

How viral cell tropism, determined by the receptor used, can affect the disease outcome in acute and chronic virus infection is a major subject under extensive investigation in Virology. To understand the mechanism which causes human diseases by viruses, that is, viral pathogenesis, we have studied various aspects of virus infection at a cell/tissue level or using animal models. In this context, the recent development of reverse genetics allows us to visualize virus-infected cells/tissues or even the virus itself. By applying such manipulated viruses to animal models, it is also possible to analyze the dynamics of virus infection *in vivo*.

In this Research Topic, we selected on studies connecting virus receptor usage and the pathogenesis of various viruses causing acute or chronic infection. Eventually, it could expand to cover the receptor-pathogenesis relationship in various acute and chronic virus infection. This research topic comprises an original research article on HIV-1, two opinions articles on the hepatitis C virus (HCV) and norovirus, while the remaining review articles on HTVL-1, measles virus (MV), mouse hepatitis virus (MHV), influenza virus, HCV, and enterovirus (EV) provide overviews on various aspects of viral pathogenesis. In all these review/opinion articles, at least one comprehensive table or figure is incorporated so that readers who are unfamiliar with these viruses can get a message at a glance.

With regards to the cell tropism of HIV-1, Terahara et al. (2012) presented his recent study using CCR5-tropic and CXCR4-tropic HIV-1 with distinct fluorescent reporter. These HIV-1s allowed us to detect HIV-infected cells at a different stage of infection and to evaluate the level of virus replication in $CD4^+$ T cells with distinct differentiation phenotype including $CCR5^+$ memory. In contrast, a receptor for HTLV-1 and related pathogenesis is still intriguing issue, which is described by Hoshino (2012) in his extensive review.

The two reviews on the MV (Kato et al., 2012; Takeda et al., 2012) were published at a very appropriate time as a third receptor for MV entry into epithelial cells, nectin 4, had just been discovered (Muhlebach et al., 2011; Noyce et al., 2011). Here, Kato et al. (2012) focused on the receptor usage of MV *in vivo* which may influences the disease outcome using monkey models, while Takeda et al. (2012) discussed about the dual-tropic nature of MV using SLAM and nectin 4 expressed in immune cells and epithelial cells, respectively.

Ito et al. (2012) addressed the importance of B cells as a reservoir for persistent HCV infection. In two reviews on HCV, Moriishi and Matsuura (2012) overviewed a current research focus on lipid components for the HCV pathogenesis, while Shoji et al. (2012) discussed about glucose metabolic disorders associated with HCV infection.

Nishimura and Shimizu (2012) and Yamayoshi et al. (2012), both of whom successfully identified two novel receptors for EV, overviewed the current knowledge about receptor usage and various diseases associated with EV infection. For the coronavirus, Taguchi and Hirai-Yuki (2012) overviewed studies on the receptor and related cellular factors for MHV, which may contribute to the mouse susceptibility to MHV infection.

As regards to the virus recognizing sugar moieties, Ramos and Fernandez-Sesma (2012) provided insights about the interaction of influenza A virus with sialic acid receptors on immune cells with special reference to the innate immune response. Shirato (2012) described about the norovirus with distinct genotypes which recognize a specific structure of sugar chain.

We will learn by these articles the fact that to identify a receptor is the first important step to know a virus, but many questions remain in order to fully understand human diseases caused by viruses. I would like to express my cordial thanks to all the contributors for this topic. I hope readers find the content interesting, but most importantly, that the information will prove very useful for future research.

REFERENCES

Hoshino, H. (2012). Cellular factors involved in HTLV-1 entry and pathogenicity. *Front. Microbiol.* 3:222. doi: 10.3389/fmicb.2012.00222

Ito, M., Kusunoki, H., and Mizuochi, T. (2012). Peripheral B cells as reservoirs for persistent HCV infection. *Front. Microbiol.* 2:177. doi: 10.3389/fmicb.2011.00177

Kato, S. I., Nagata, K., and Takeuchi, K. (2012). Cell tropism and pathogenesis of measles virus in monkeys. *Front. Microbiol.* 3:14. doi: 10.3389/fmicb.2012.00014

Moriishi, K., and Matsuura, Y. (2012). Exploitation of lipid components by viral and host proteins for hepatitis C virus infection. *Front. Microbiol.* 3:54. doi: 10.3389/fmicb.2012.00054

Muhlebach, M. D., Mateo, M., Sinn, P. L., Prufer, S., Uhlig, K. M., Leonard, V. H., Navaratnarajah, C. K., Frenzke, M., Wong, X. X., Sawatsky, B., Ramachandran, S., McCray, P. B. Jr., Cichutek, K., von Messling, V., Lopez, M., and Cattaneo, R.

(2011). Adherens junction protein nectin-4 is the epithelial receptor for measles virus. *Nature* 480, 530–533.

Nishimura, Y., and Shimizu, H. (2012). Cellular receptors for human enterovirus species a. *Front. Microbiol.* 3:105. doi: 10.3389/fmicb.2012.00105

Noyce, R. S., Bondre, D. G., Ha, M. N., Lin, L. T., Sisson, G., Tsao, M. S., and Richardson, C. D. (2011). Tumor cell marker PVRL4 (nectin 4) is an epithelial cell receptor for measles virus. *PLoS Pathog.* 7, e1002240. doi: 10.1371/journal.ppat.1002240

Ramos, I., and Fernandez-Sesma, A. (2012). Cell receptors for influenza a viruses and the innate immune response. *Front. Microbiol.* 3:117. doi: 10.3389/fmicb.2012.00117

Shirato, H. (2012). Norovirus Recognition Sites on Histo-Blood Group Antigens. *Front. Microbiol.* 3:177. doi: 10.3389/fmicb.2012.00177

Shoji, I., Deng, L., and Hotta, H. (2012). Molecular mechanism of hepatitis C virus-induced glucose metabolic disorders. *Front. Microbiol.* 2:278. doi: 10.3389/fmicb.2011.00278

Taguchi, F., and Hirai-Yuki, A. (2012). Mouse hepatitis virus receptor as a determinant of the mouse susceptibility to MHV Infection. *Front. Microbiol.* 3:68. doi: 10.3389/fmicb.2012.00068

Takeda, M., Tahara, M., Nagata, N., and Seki, F. (2012). Wild-Type Measles Virus is Intrinsically Dual-Tropic. *Front. Microbiol.* 2:279. doi: 10.3389/fmicb.2011.00279

Terahara, K., Yamamoto, T., Mitsuki, Y. Y., Shibusawa, K., Ishige, M., Mizukoshi, F., Kobayashi, K., and Tsunetsugu-Yokota, Y. (2012). Fluorescent Reporter Signals, EGFP, and DsRed, Encoded in HIV-1 Facilitate the Detection of Productively Infected Cells and Cell-Associated Viral Replication Levels. *Front. Microbiol.* 2:280. doi: 10.3389/fmicb.2011.00280

Yamayoshi, S., Fujii, K., and Koike, S. (2012). Scavenger receptor b2 as a receptor for hand, foot, and mouth disease and severe neurological diseases. *Front. Microbiol.* 3:32. doi: 10.3389/fmicb.2012.00032

Received: 20 July 2012; accepted: 23 July 2012; published online: 08 August 2012.
*Citation: Tsunetsugu-Yokota Y and Terahara K (2012) Receptor usage and the pathogenesis in acute and chronic virus infections. Front. Microbio. **3**:289. doi: 10.3389/fmicb.2012.00289*
This article was submitted to Frontiers in Virology, a specialty of Frontiers in Microbiology.

JVI Journals.ASM.org

HIV-1 Infection *Ex Vivo* Accelerates Measles Virus Infection by Upregulating Signaling Lymphocytic Activation Molecule (SLAM) in CD4$^+$ T Cells

Yu-ya Mitsuki,[a] Kazutaka Terahara,[a] Kentaro Shibusawa,[a] Takuya Yamamoto,[b] Takatsugu Tsuchiya,[a] Fuminori Mizukoshi,[a] Masayuki Ishige,[a,c] Seiji Okada,[c] Kazuo Kobayashi,[a] Yuko Morikawa,[d] Tetsuo Nakayama,[e] Makoto Takeda,[f] Yusuke Yanagi,[g] and Yasuko Tsunetsugu-Yokota[a]

Department of Immunology, National Institute of Infectious Diseases, Shinjuku-ku, Tokyo, Japan[a]; Immunology Laboratory, Vaccine Research Center, National Institute of Allergy and Infectious Diseases, National Institutes of Health, Bethesda, Maryland, USA[b]; Center for AIDS Research, Kumamoto University, Kumamoto, Japan[c]; Laboratory of Viral Infection II, Kitasato Institute for Life Science, Kitasato University, Tokyo, Japan[d]; Laboratory of Viral Infection I, Kitasato Institute for Life Science, Kitasato University, Tokyo, Japan[e]; Department of Virology III, National Institute of Infectious Diseases, Tokyo, Japan[f]; and Department of Virology, Faculty of Medicine, Kyushu University, Fukuoka, Japan[g]

Measles virus (MV) infection in children harboring human immunodeficiency virus type 1 (HIV-1) is often fatal, even in the presence of neutralizing antibodies; however, the underlying mechanisms are unclear. Therefore, the aim of the present study was to examine the interaction between HIV-1 and wild-type MV (MVwt) or an MV vaccine strain (MVvac) during dual infection. The results showed that the frequencies of MVwt- and MVvac-infected CD4$^+$ T cells within the resting peripheral blood mononuclear cells (PBMCs) were increased 3- to 4-fold after HIV-1 infection, and this was associated with a marked upregulation of signaling lymphocytic activation molecule (SLAM) expression on CD4$^+$ T cells but not on CD8$^+$ T cells. SLAM upregulation was induced by infection with a replication-competent HIV-1 isolate comprising both the X4 and R5 types and to a lesser extent by a pseudotyped HIV-1 infection. Notably, SLAM upregulation was observed in HIV-infected as well as -uninfected CD4$^+$ T cells and was abrogated by the removal of HLA-DR$^+$ cells from the PBMC culture. Furthermore, SLAM upregulation did not occur in uninfected PBMCs cultured together with HIV-infected PBMCs in compartments separated by a permeable membrane, indicating that no soluble factors were involved. Rather, CD4$^+$ T cell activation mediated through direct contact with dendritic cells via leukocyte function-associated molecule 1 (LFA-1)/intercellular adhesion molecule 1 (ICAM-1) and LFA-3/CD2 was critical. Thus, HIV-1 infection induces a high level of SLAM expression on CD4$^+$ T cells, which may enhance their susceptibility to MV and exacerbate measles in coinfected individuals.

The attenuated measles virus (MV) vaccine has greatly reduced the morbidity and mortality of measles in industrialized countries. However, measles is still a leading cause of death among children in developing countries, especially in sub-Saharan Africa, where almost 90% of global pediatric human immunodeficiency virus type 1 (HIV-1) infections occur (http://apps.who.int/ghodata/). Because both HIV-1 and MV cause immunosuppression, it is conceivable that coinfection with HIV-1 and MV increases the risk of disease progression (17). In fact, an observational study of hospitalized children in Zambia showed that the fatality rate increased among HIV-1-infected children with measles (18).

The low levels of neutralizing antibodies in HIV-1-infected children may explain the high mortality of measles. The measles vaccine is only weakly immunogenic in HIV-1-infected children, inducing only low levels of neutralizing antibody, which decline rapidly (17). However, a recent large-scale prospective study in Zambia conducted by Moss et al. reported a good initial antibody response to measles vaccine in both HIV-1-infected and -uninfected children (19). Moreover, to understand the impact of HIV-1 infection on the clinical manifestation of measles, Permar et al. conducted a study using MV-vaccinated or -unvaccinated rhesus monkeys that are chronically infected with a simian immunodeficiency virus (24). They monitored the virological and immunological status of the monkeys after MV challenge and found that the clinical manifestation of measles occurs even in monkeys with high titers of vaccine-induced MV neutralizing antibody. This finding implies that the presence of neutralizing antibody alone is not sufficient protection from measles in HIV-1-infected individuals. Therefore, it is highly likely that an as yet unknown factor(s)/mechanism(s) affected by HIV-1 is involved in the exacerbation of measles in HIV-1-infected individuals.

Some studies analyzed the interaction between MV and HIV-1 *in vitro*. Garcia et al. studied HIV-1 replication in peripheral blood mononuclear cells (PBMCs) coinfected with MV and found that MV-induced inhibition of lymphocyte proliferation suppresses HIV-1 replication, but without any apparent increase in the production of chemokines or any other soluble factors in coinfected cultures (7). In a more recent study, the same group demonstrated that the cell cycle progression of T cells, which is required for efficient HIV-1 replication, was blocked by MV (8); however, it is still not clear whether HIV-1 affects MV infection directly or indirectly.

Understanding the impact of HIV-1 infection on MV infection

Received 28 October 2011 **Accepted** 10 April 2012
Published ahead of print 24 April 2012
Address correspondence to Yasuko Tsunetsugu-Yokota, yyokota@nih.go.jp.
Supplemental material for this article may be found at http://jvi.asm.org/.

doi:10.1128/JVI.06681-11

and replication is important both for developing successful strategies for measles eradication and for HIV-1 control. The receptor for wild-type MV has been identified to be signaling lymphocytic activation molecule (SLAM; also known as CD150), and attenuated vaccine strains can utilize both SLAM and CD46 (4). Recently, nectin4 was also identified as an MV receptor that is important for MV to spread into epithelial cells and release viral particles from the apical membrane into the lumen of the respiratory tract (20, 21). However, SLAM remains a major receptor of MV in lymphoid organs and plays an important role in a systemic MV infection. Therefore, the aim of the present study was to investigate the course of MV infection in HIV-1-infected PBMCs *ex vivo* at the level of the individual cell, focusing on SLAM expression. The results presented here showed that HIV-1 replication in resting PBMCs induces the upregulation of SLAM expression on $CD4^+$ T cells in a manner that is dependent on cell-to-cell contact, resulting in higher levels of MV infection.

MATERIALS AND METHODS

Cell preparation. Human peripheral blood samples were collected from healthy donors after receiving written informed consent. Sample collection was approved by the institutional ethical committee of the National Institute of Infectious Diseases (Tokyo, Japan). PBMCs were separated by Ficoll-Hypaque density gradient centrifugation (Lymphosepal; IBL, Gunma, Japan). T cells were isolated using a total T cell enrichment kit (StemCell Technologies, Vancouver, BC, Canada), after depletion of $CD14^+$ cells. For monocyte depletion, $CD14^+$ cells were depleted from PBMCs using magnetically activated cell sorting (MACS) with CD14 microbeads (Miltenyi Biotec, Cologne, Germany). For B cell and HLA-DR^+ cell depletion, PBMCs were incubated with biotin-labeled anti-CD19 (BioLegend, San Diego, CA) and biotin-labeled anti-HLA-DR (BioLegend) antibodies, respectively, followed by positive selection using anti-biotin tetrameric antibody complex (TAC), magnetic colloid, and an EasySep magnet (all from StemCell Technologies).

Preparation of virus stock. To prepare HIV-1 clones HIV-$1_{NL\text{-}E}$, HIV-$1_{NLAD8\text{-}E}$, and HIV-$1_{NL\text{-}D}$, human 293T embryonic kidney cells seeded at a density of 7×10^6 cells/15-cm dish were transfected with 30 μg of pNL-E, pNLAD8-E, and pNL-D, respectively, using the calcium phosphate precipitation method as described previously (29). To prepare HIV-1 pseudotyped with vesicular stomatitis virus glycoprotein (HIV-1/VSV-G), 293T cells were cotransfected with 36 μg of pNL-EdENV (pNL-E with an *env*-inactivating mutation) and 4 μg of pVSV-G per 7×10^6 cells. At 2 days posttransfection, the culture supernatant was collected, filtrated, and frozen at −80°C. The amounts of viruses in each culture supernatant were measured using an in-house HIV-1 Gag p24 enzyme-linked immunosorbent assay.

To prepare green fluorescent protein (GFP)-expressing wild-type (IC323-EGFP) (12) or vaccine strain (GFP-MVAIK) (6) MV, 1×10^7 human SLAM-expressing Vero cells (Vero/hSLAM) cells were infected with 1×10^5 PFU of each virus (multiplicity of infection [MOI] = 0.01) for 2 h, washed, and then grown in Dulbecco's modified Eagle medium (DMEM; Gibco, Carlsbad, CA) supplemented with 2% heat-inactivated fetal bovine serum (FBS). Infected cells were harvested when approximately 80% cytotoxicity was observed. Cells were then frozen and thawed three times and sonicated for 10 s to release the cell-bound viruses. The titer of measles virus was measured using a plaque assay, described in the following section.

Titration of MV. MV was titrated as described previously (26). In brief, monolayers of 2×10^5 Vero/hSLAM cells grown in 12-well plates were infected with serially diluted wild-type MV (MVwt) or an attenuated MV vaccine strain (MVvac). After removal of viruses, the cells were overlaid with DMEM supplemented with 2% methylcellulose and 2% FBS. At day 5 postinfection, cells were stained with 5% neutral red, the numbers of plaques were counted, and the numbers of PFU/ml were calculated.

HIV-1 and MV infection. For HIV-1 infection, untreated PBMCs or PBMCs depleted of either $CD14^+$ monocytes, $CD19^+$ B cells, or HLA-DR^+ cells or purified T cells (1×10^6 cells) were infected with 100 ng of p24 of either HIV-$1_{NL\text{-}E}$, HIV-$1_{NL\text{-}D}$, HIV-$1_{NLAD8\text{-}E}$, or HIV-1/VSV-G for 2 h, washed three times with RPMI 1640 (RPMI), and then cultured in RPMI supplemented with 5% heat-inactivated human serum (P-RPMI), penicillin (100 μg/ml), and streptomycin (100 μg/ml). At day 3 postinfection, the culture medium was changed to 5% P-RPMI supplemented with interleukin-2 (IL-2; 50 U/ml) and then cultured for 2 days.

For MV infection, HIV-$1_{NL\text{-}D}$-infected and -uninfected PBMCs (1×10^6 cells) were mock infected or infected with 5×10^4 PFU of either MVwt or MVvac for 2 h at day 5 after HIV infection, washed three times with RPMI, and then cultured in 5% P-RPMI for 2 days.

Flow cytometry. Cells were stained with a suitable combination of fluorescence-labeled monoclonal antibodies (MAbs): Pacific Blue-labeled anti-CD4 (eBioscience, San Diego, CA), allophycocyanin (APC)-Cy7-labeled anti-CD8 (eBioscience), peridinin chlorophyll protein-labeled anti-CD3 (R&D Systems, Inc., Minneapolis, MN), APC-labeled anti-CD14 (R&D Systems), phycoerythrin (PE)-labeled anti-SLAM (eBioscience), and PE-Cy7-labeled anti-CD19 (BioLegend). Dead cells were visualized using a LIVE/DEAD fixable dead cell stain kit (Invitrogen, Carlsbad, CA). HIV-1- and/or MV-infected cells were analyzed using flow cytometry (FACSCant II flow cytometer; BD Bioscience, Pharmingen, CA) and a FACSDiva flow cytometer (BD Bioscience) or Flowjo software (Tree Star, San Carlos, CA).

Detection of cytokines. The levels of gamma interferon (IFN-γ), IL-1β, IL-2, IL-5, IL-10, tumor necrosis factor alpha (TNF-α), and TNF-β in the culture supernatant of the HIV-1-infected or mock-infected PBMC cultures were measured using a FlowCytomix human Th1/Th2 11plex kit (Bender MedSystems, Vienna, Austria), according to the manufacturer's protocol, at day 5 postinfection. The minimum detection levels for each cytokine were as follows: IFN-γ, 1.6 pg/ml; IL-1β, 4.2 pg/ml; IL-2, 16.4 pg/ml; IL-4, 20.8 pg/ml; IL-5, 1.6 pg/ml; IL-6, 1.2 pg/ml; IL-8, 0.5 pg/ml; IL-10, 1.9 pg/ml; IL-12 p70, 1.5 pg/ml; TNF-α, 3.2 pg/ml; and TNF-β, 2.4 pg/ml. Results were calculated using FlowCytomix Pro software (Bender MedSystems).

Transwell assay. HIV-1-infected or -uninfected PBMCs were cultured in the top chamber of a transwell plate (pore size, 0.4 μm; Costar; Corning, Corning, NY). HIV-1-uninfected PBMCs were placed on the bottom chamber and cultured for 5 days.

Blocking of antibodies against cell adhesion molecules. An isotype control IgG1 (PeproTech Inc., Rocky Hill, NJ) or serial dilutions of anti-leukocyte function-associated molecule 1α (anti-LFA-1α) or anti-LFA-3 MAbs (serially diluted from 10 μg/ml) were added to HIV-1-infected PBMC cultures just after 2 h of infection to analyze the effect of cell-to-cell contact on SLAM upregulation. Anti-LFA-1α and anti-LFA-3 MAbs were prepared from hybridomas kindly provided by Hideo Yagita (Juntendo University, Tokyo, Japan).

Statistical analysis. Because of the limited sample size, each experiment was performed once per donor. Data obtained from less than three donors were excluded from the statistical analysis. The significance of the data was evaluated by the Mann-Whitney U test, by the Tukey multiple-comparison test, or by use of the Pearson correlation coefficient on the basis of the normality and variance of the data using GraphPad Prism software (version 4.0; GraphPad Software, San Diego, CA). P values of <0.05 were considered statistically significant.

RESULTS

HIV-1 infection enhances the infectivity of coinfected MV *ex vivo*. First, the consequences of coinfection of PBMCs with HIV-1 and MV were analyzed at the single-cell level using flow cytometry. DsRed-expressing ($DsRed^+$) HIV-$1_{NL\text{-}D}$- or mock-infected PBMCs were coinfected with GFP-expressing (GFP^+) MVwt or

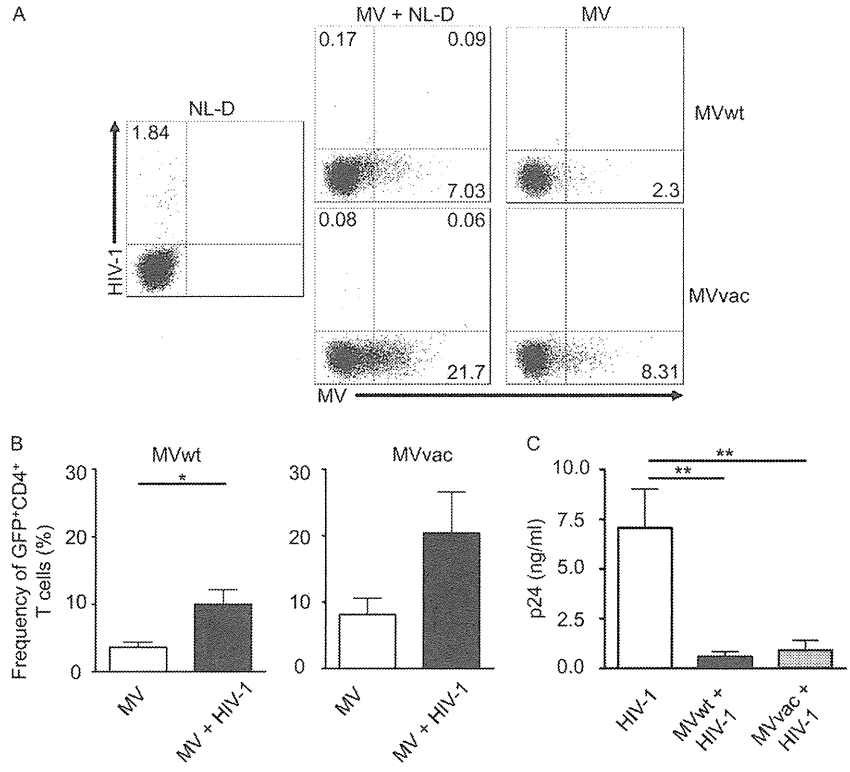

FIG 1 Effect of HIV-1 infection on MV infection in an *ex vivo* HIV-1/MV coinfection model. PBMCs were coinfected with HIV-1_{NL-D} and/or either MVwt or MVvac, and the infected cells were analyzed. (A) Representative flow cytometry plots showing MVwt- or MVvac-infected $CD4^+$ T cells. (B) Cumulative data showing the frequency of MVwt- or MVvac-infected $CD4^+$ T cells. The bars represent the mean ± SEM ($n = 7$). *P* values were calculated using the Mann-Whitney U test. *, $P < 0.05$. (C) Levels of p24 antigen in culture supernatants of HIV-1 and/or MV-infected PBMCs. The bars represent the mean ± SEM ($n = 5$). *P* values were calculated using one-way analysis of variance followed by the Tukey multiple-comparison test. **, $P < 0.01$.

MVvac at day 5. Two days later, HIV- and/or MV-infected cells were analyzed. As shown in Fig. 1A, HIV-1_{NL-D}-infected and MV-infected cells were identified as $DsRed^+$ and GFP^+ cells, respectively. In the case of MVwt infection, the frequency of MVwt-infected $CD4^+$ T cells within the HIV-1_{NL-D}-infected PBMC population (9.96% ± 2.45%) was significantly higher than that in the MV-only-infected PBMC population (3.60% ± 0.77%) ($P = 0.0175$; $n = 7$; Fig. 1B, left). Likewise, in the case of MVvac infection, the frequency of MVvac-infected $CD4^+$ T cells tended to be higher within the HIV-1_{NL-D}-infected PBMC population (20.42% ± 6.20%) than within the MV-only-infected PBMC population (8.14% ± 2.45%), although the result was not statistically significant ($P = 0.1158$; $n = 7$; Fig. 1B, right). These results indicated that HIV-1 infection enhances MV infection in PBMCs. It should be noted that the HIV-infected $CD4^+$ T cell population disappeared upon MV infection (from 1.84% to 0.26% and 0.14% for MVwt and MVvac, respectively), and the doubly infected $CD4^+$ T cell population was rarely visible (Fig. 1A). Although we used the same MOI, the percentage of MV-infected T cells was always higher in MVvac infection than in MVwt infection. This is probably due to the wider tropism of MVvac, which utilizes both SLAM and CD46 as receptors (4).

The level of HIV-1 Gag p24 in the culture supernatant was also significantly reduced by coinfection with either MVwt or MVvac compared with that observed after infection with HIV-1_{NL-D} alone ($P < 0.01$; $n = 5$; Fig. 1C). These results are consistent with those reported previously; i.e., MV infection inhibits the replication of HIV-1 (7, 8, 10).

SLAM expression on $CD4^+$ T cells is induced by HIV-1 infection. Because both MVwt and MVvac utilize SLAM as a receptor (5, 22), SLAM expression was examined in HIV-1-infected PBMCs. PBMCs were infected with either CXCR4-tropic HIV-1_{NL-E}, CCR5-tropic HIV-$1_{NLAD8-E}$, or HIV-1/VSV-G, all of which express GFP, and were then cultured for 5 days without additional stimulation (apart from the addition of IL-2). It is noteworthy that, regardless of HIV-1 infection, SLAM expression was slightly increased under these culture conditions at day 5 (basal increase), and this basal increase varied among individuals (5.17 ± 2.63% at day 0 to 8.81% ± 2.00% at day 5; $n = 7$). Therefore, the net increase in the frequency of $SLAM^{hi}$ $CD4^+$ or $SLAM^{hi}$ $CD8^+$ T cells was calculated by subtracting their respective basal levels of increase. Induction of SLAM expression on $CD8^+$ T cells was low and did not increase statistically significantly with HIV-1 infection (Fig. 2A, bottom, and B, right). However, importantly, both the level of SLAM expression and the frequency of $SLAM^{hi}$ $CD4^+$ T cells increased after infection with HIV-1, and increased SLAM expression was observed in HIV-1-infected (GFP^+) as well as in uninfected $CD4^+$ T cells (Fig. 2A, top). Because the net increase in SLAM expression varied between donors, PBMCs from 10 donors were examined. The frequency of $SLAM^{hi}$ $CD4^+$ T cells markedly increased in the HIV-1_{NL-E}-infected cultures (8.79% ± 1.47%), while the frequency in HIV-1/VSV-G-infected cultures increased only slightly (2.52% ± 0.58%). This difference between HIV-1_{NL-E}- and HIV-1/VSV-G-infected cultures was statistically significant ($P < 0.01$; $n = 10$; Fig. 2B). Of note, HIV-1/VSV-G-infected

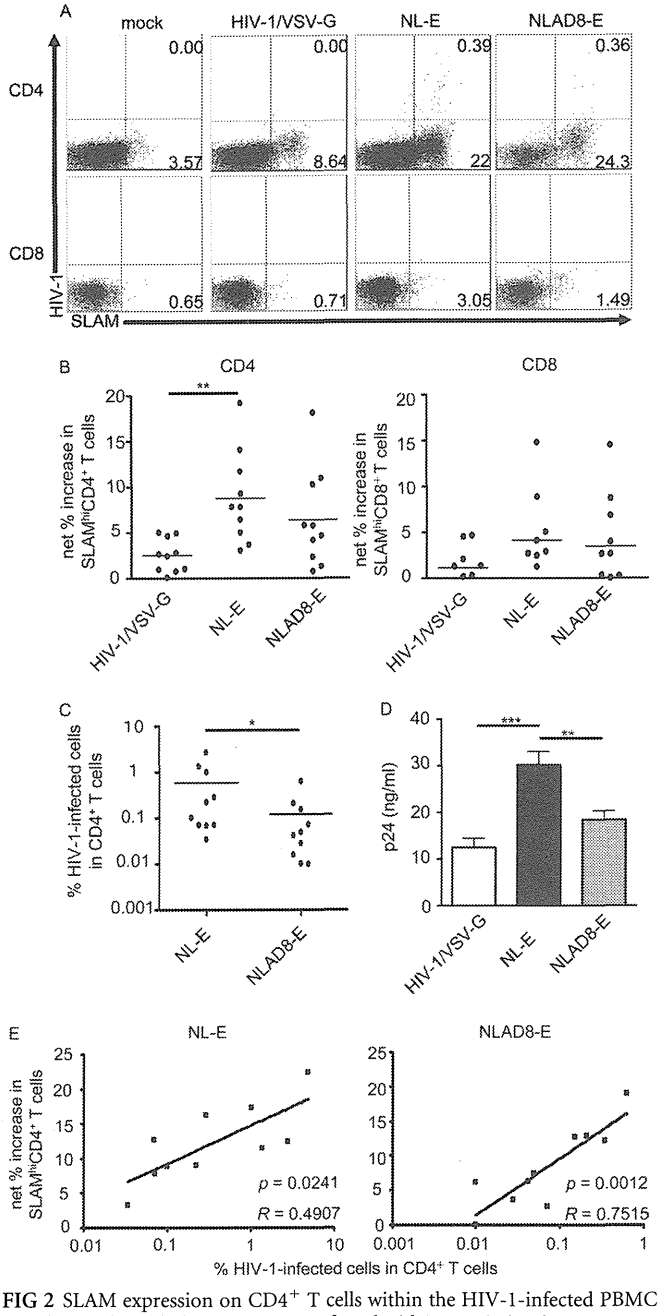

FIG 2 SLAM expression on $CD4^+$ T cells within the HIV-1-infected PBMC population. (A and B) PBMCs were infected with HIV-1/VSV-G, HIV-1_{NL-E}, or HIV-$1_{NLAD8-E}$, and SLAM expression on $CD4^+$ T cells was analyzed. (A) Representative flow cytometry plots showing SLAM expression on $CD4^+$ T cells and $CD8^+$ T cells. (B) Cumulative data showing the percent increase in the frequency of $SLAM^{hi}$ $CD4^+$ and $SLAM^{hi}$ $CD8^+$ T cells from 10 donors. *P* values were calculated using one-way analysis of variance followed by the Tukey multiple-comparison test. **, $P < 0.01$. (C) Cumulative data showing the frequency of HIV-1-infected $CD4^+$ T cells from 10 donors. *P* values were calculated using the Mann-Whitney U test. *, $P < 0.05$. (D) Levels of p24 antigen in culture supernatants of HIV-1-infected PBMCs. The bars represent the mean ± SEM ($n = 10$). *P* values were calculated using one-way analysis of variance followed by the Tukey multiple-comparison test. **, $P < 0.01$; ***, $P < 0.001$. (E) Correlation between the frequency of HIV-1_{NL-E}- and HIV-$1_{NLAD8-E}$-infected $CD4^+$ T cells and the percent increase in the frequency of $SLAM^{hi}$ $CD4^+$ T cells from 10 donors. Correlation statistics were analyzed using the Pearson correlation.

(GFP^+) cells were scarcely detectable under these conditions, probably reflecting the low transduction efficiency of VSV-pseudotyped lentivirus in unstimulated T cells. A marked upregulation of SLAM expression induced by HIV-$1_{NLAD8-E}$ infection was also observed in some donors, but the difference between HIV-$1_{NLAD8-E}$- and HIV-1/VSV-G-infected cultures was not statistically significant (Fig. 2B). This probably reflects the variable number and low frequency of $CCR5^+$ $CD4^+$ T cells (5 to 10% of $CD4^+$ T cells), which are a target of CCR5-tropic HIV-$1_{NLAD8-E}$, in donor PBMCs. As expected, the frequency of HIV-1_{NL-E}-infected $CD4^+$ T cells (0.88% ± 0.28%) was higher than that of HIV-$1_{NLAD8-E}$-infected $CD4^+$ T cells (0.19% ± 0.01%) ($P = 0.0433$; $n = 10$; Fig. 2C). In parallel with the high frequency of $SLAM^{hi}$ $CD4^+$ T cells, the levels of p24 were the highest in the culture supernatants of HIV-1_{NL-E}-infected cultures compared to other HIV-1-infected cultures (Fig. 2D). There was a significant correlation between the frequency of HIV-1-infected $CD4^+$ T cells and that of $SLAM^{hi}$ $CD4^+$ T cells in both HIV-1_{NL-E}-infected ($R = 0.4907$, $P = 0.0241$; $n = 10$) and HIV-$1_{NLAD8-E}$-infected ($R = 0.7517$; $P = 0.0012$; $n = 10$) cultures (Fig. 2E).

To determine whether the replication of HIV-1 was required for SLAM upregulation, PBMCs were infected with a 20-fold higher dose of HIV-1/VSV-G. The frequency of GFP^+ $CD4^+$ T cells and $SLAM^{hi}$ $CD4^+$ T cells under these conditions was identical to that seen in HIV-1_{NL-E}-infected PBMCs (see Fig. S1 in the supplemental material). Taken together, these results indicated that HIV-1 replication is not essential but that higher and/or persistent levels of HIV-1 are involved in the upregulation of SLAM expression on $CD4^+$ T cells.

All subsequent studies were carried out using CXCR4-tropic HIV-1_{NL-E}.

SLAM upregulation by HIV-1 infection is not caused by direct infection of $CD4^+$ T cells. Despite the fact that HIV-1 infection enhanced SLAM expression on $CD4^+$ T cells, upregulation was more obvious in HIV-1-uninfected $CD4^+$ T cells (Fig. 2A). To further test the importance of direct HIV-1 infection of $CD4^+$ T cells for SLAM upregulation, T cells were enriched from PBMCs. PBMCs and T cells were separately infected with HIV-1_{NL-E}, and the expression of SLAM on $CD4^+$ T cells was analyzed after 5 days of culture. A representative result from six individuals is shown in Fig. 3A, and plots from all six individuals are shown, with averages, in Fig. 3B. The majority of HIV-1_{NL-E}-infected $CD4^+$ T cells in the purified T cell cultures were SLAM-dull (Fig. 3A), and the net increase in the frequency of $SLAM^{hi}$ $CD4^+$ T cells (2.87% ± 1.04%) was much lower than that in the PBMC cultures (13.00% ± 3.72%) ($P < 0.01$; $n = 6$; Fig. 3B). To examine in more detail which cell population within the PBMCs contributed to the upregulation of SLAM by HIV-1 infection, whole PBMCs and those depleted of either $CD14^+$ monocytes, $CD19^+$ B cells, or $HLA\text{-}DR^+$ cells were infected with HIV-1_{NL-E}. Cell depletion was evaluated by flow cytometry (Fig. 3C). The removal of $HLA\text{-}DR^+$ cells resulted in depletion of both monocytes and B cells (Fig. 3C, lower right). Of note, a minor population of CD123-, CD141-, and/or CD303-expressing cells (peripheral dendritic cells [pDCs] and conventional dendritic cells [DCs]) were also removed by depletion of $HLA\text{-}DR^+$ cells (data not shown). There were no significant differences in the increase in $SLAM^{hi}$ $CD4^+$ T cells among monocyte- and B cell-depleted PBMCs compared to whole PBMCs following HIV-1 infection in four donors; the relative increases in monocyte- and B cell-depleted PBMCs compared to

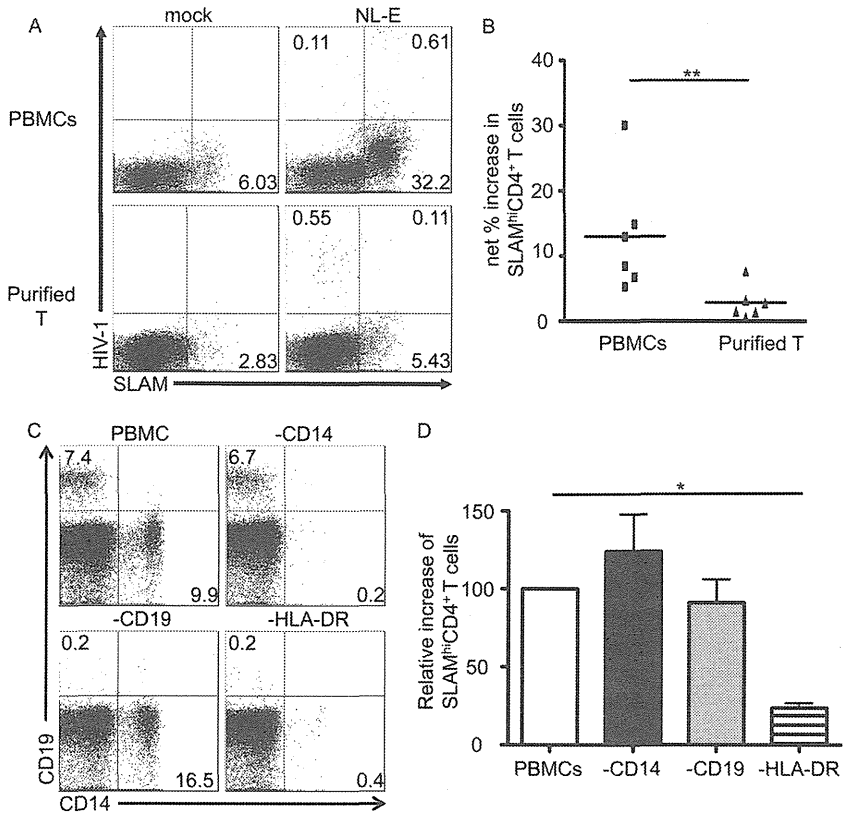

FIG 3 Comparison of the levels of SLAM upregulation on $CD4^+$ T cells induced by HIV-1 infection in the presence or absence of non-T cells. (A and B) Purified T cells and PBMCs were separately infected with HIV-1_{NL-E}. (A) Representative flow cytometry plots showing SLAM expression on $CD4^+$ T cells. (B) Cumulative data showing the percent increase in $SLAM^{hi}$ $CD4^+$ T cells. The bars represent the mean ± SEM ($n = 6$). *P* values were calculated using the Mann-Whitney U test. **, $P < 0.01$. (C and D) PBMCs were infected with HIV-1_{NL-E} after removal of monocytes, B cells, or $HLA\text{-}DR^+$ cells. (C) Representative flow cytometry plot evaluating the depletion of monocytes, B cells, or $HLA\text{-}DR^+$ cells. (D) Cumulative data showing the relative increase in the frequency of $SLAM^{hi}$ $CD4^+$ T cells. The increase in the frequency of $SLAM^{hi}$ $CD4^+$ T cells by HIV-1 infection in the PBMC population was set to 100%. The bars represent the mean ± SEM ($n = 4$). *P* values were calculated using one-way analysis of variance followed by the Tukey multiple-comparison test. *, $P < 0.05$.

whole PBMCs (set at 100%) were 124.1% ± 23.68% and 91.19% ± 14.84%, respectively ($n = 4$). In contrast, SLAM expression was significantly repressed in $HLA\text{-}DR^+$ cell-depleted PBMCs following HIV-1 infection (relative increase, 23.65% ± 3.13%; $n = 4$). Taken together, these results indicated that a population of HLA-DR-expressing cells, including DCs, but not monocytes and B cells, is involved in the upregulation of SLAM by HIV-1 infection.

Role of cytokines in induction of SLAM expression during HIV infection. SLAM expression on T cells and DCs is upregulated by IFN-γ (9) and IL-1β (14), respectively. Therefore, the levels of 11 cytokines (IFN-γ, IL-1β, IL-2, IL-4, IL-5, IL-6, IL-8, IL-10, IL-12 p70, TNF-α, and TNF-β) in the culture supernatants of HIV-1_{NL-E}-infected and -uninfected PBMCs were measured at day 5. The results showed that the production of IFN-γ, IL-1β, and TNF-α in HIV-1_{NL-E}-infected PBMCs was significantly higher than that in uninfected PBMCs ($P = 0.0006$, 0.0023, and 0.0041, respectively; $n = 4$; Fig. 4A). The levels of IL-2, IL-4, IL-5, IL-6, IL-8, IL-10, IL-12 p70, and TNF-β were low or undetectable, irrespective of HIV-1 infection (data not shown). SLAM upregulation on $CD4^+$ T cells was not affected, when HIV-1_{NL-E}-infected PBMCs were cultured in the absence or presence of anti-IFN-γ blocking MAb (data not shown). Furthermore, SLAM upregulation was not observed in PBMC cultures in the presence of recombinant IFN-γ (data not shown).

To test the potential contribution of any soluble factors produced in HIV-1-infected PBMC cultures, we performed a transwell assay. HIV-1_{NL-E}-infected PBMCs were seeded into the top chamber of the transwell, and uninfected PBMCs were placed in the bottom chamber. The cells were then cultured for 5 days. A representative result is shown in Fig. 4B. SLAM was markedly upregulated in HIV-1_{NL-E}-infected PBMCs in the top chamber (net increase, 32.81%; Fig. 4B, upper right), whereas upregulation was less obvious in uninfected PBMCs in the bottom chamber (net increase, 3.35%; Fig. 4B, lower right). The result was reproduced using PBMCs from eight separate donors, and the difference was statistically significant (bottom chamber, 1.07% ± 0.80%; top chamber, 9.08% ± 4.60%; $P < 0.001$; $n = 5$; Fig. 4C). Thus, these data clearly show that soluble factors produced by HIV-1 infection make a minimal contribution (if any) to SLAM upregulation on $CD4^+$ T cells. Rather, cell-to-cell contact would appear to be the most important factor.

Importance of costimulatory molecules for SLAM upregulation on $CD4^+$ T cells. SLAM expression on T cells is induced by T cell receptor (TcR) stimulation with anti-CD3 antibody (3). In addition, Sheng and colleagues showed that LFA-3/CD2 interaction and, particularly, CD2 signaling are necessary but not sufficient for $CD4^+$ T cell activation (25). We showed earlier that in PBMCs, $HLA\text{-}DR^+$ cells are largely responsible for the upregulation of SLAM after HIV-1 infection (Fig. 3C). Previously, we

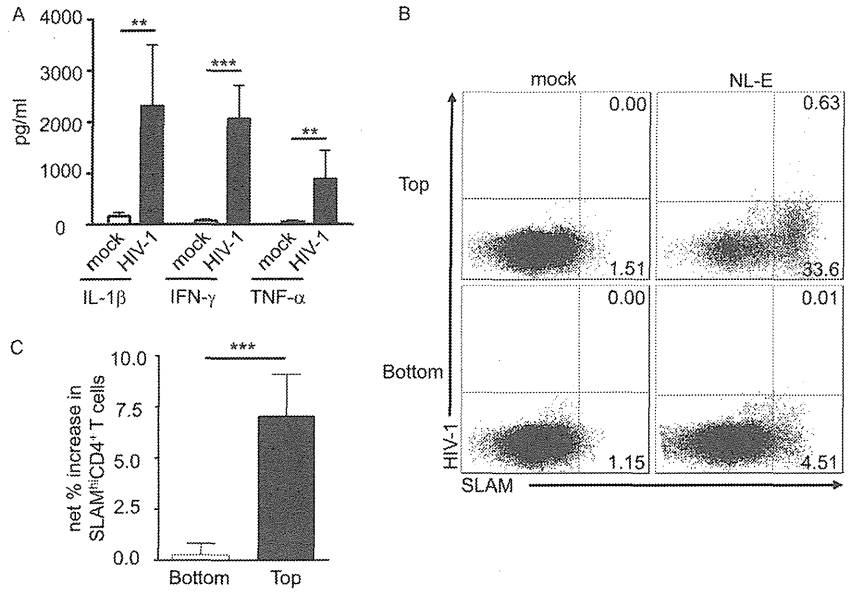

FIG 4 Impact of soluble factors on SLAM upregulation by HIV-1-infected $CD4^+$ T cells. (A) PBMCs were infected with $HIV\text{-}1_{NL\text{-}E}$, and the cytokine levels in the culture supernatants were measured. The bars represent the mean ± SEM ($n = 7$). *P* values were calculated using the Mann-Whitney U test. **, $P < 0.01$; ***, $P < 0.001$. (B and C) $HIV\text{-}1_{NL\text{-}E}$- and mock-infected PBMCs were cultured in the top chamber and uninfected PBMCs were placed in the bottom chamber of a transwell plate. (B) Representative flow cytometry plots showing SLAM expression on $CD4^+$ T cells. (C) Percent increase in the frequency of $SLAM^{hi}$ $CD4^+$ T cells. The bars represent the mean ± SEM ($n = 8$). *P* values were calculated using the Mann-Whitney U test. ***, $P < 0.001$.

showed that HIV-1 replication and expansion are associated with the activation of $CD4^+$ T cells through cell-to-cell contact with monocyte-derived DCs via costimulatory molecules such as LFA-1/intercellular adhesion molecule 1 (ICAM-1) and LFA-3/CD2 (27). We next tested the effect of blocking antibodies that inhibited these interactions on SLAM expression on $CD4^+$ T cells. $HIV\text{-}1_{NL\text{-}E}$-infected PBMCs were cultured in the absence or presence of blocking MAbs against LFA-1α and LFA-3. As shown in Fig. 5A, increased SLAM expression on $CD4^+$ T cells within the $HIV\text{-}1_{NL\text{-}E}$-infected PBMC population was inhibited by anti-LFA-1α MAb (48.81% ± 18.12%; $n = 5$) as well as by anti-LFA-3 MAb (86.58% ± 6.93%; $n = 5$), although the effect of anti-LFA-1α MAb was less pronounced and was not statistically significant at 10 μg/ml (Fig. 5B). Nevertheless, both anti-LFA-1α and anti-LFA-3 MAbs inhibited SLAM upregulation in a dose-dependent manner (Fig. 5C), and the in-

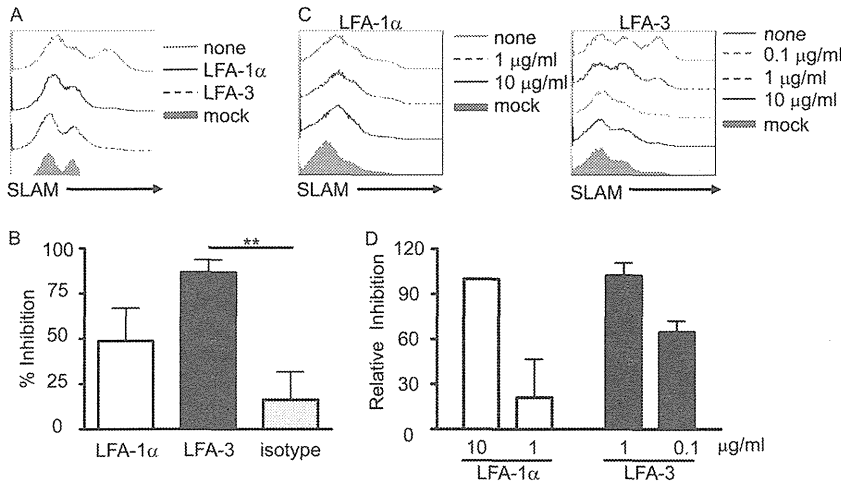

FIG 5 Role of cell-to-cell contact in SLAM upregulation on HIV-1-infected $CD4^+$ T cells. (A and B) $HIV\text{-}1_{NL\text{-}E}$-infected PBMCs were cultured in the presence of 10 μg/ml of anti-LFA-1α or anti-LFA-3 MAbs or isotype control IgG1. (A) Representative histogram showing SLAM expression on $CD4^+$ T cells. (B) Percent inhibition of the increase in the frequency of $SLAM^{hi}$ $CD4^+$ T cells. The frequency of $SLAM^{hi}$ $CD4^+$ T cells upregulated by HIV-1 infection was arbitrarily designated 100%. The bars represent the mean ± SEM ($n = 5$). *P* values were calculated using one-way analysis of variance followed by the Tukey multiple-comparison test. **, $P < 0.01$. (C and D) $HIV\text{-}1_{NL\text{-}E}$-infected PBMCs were cultured in the presence of serially diluted concentrations of anti-LFA-1α or anti-LFA-3 MAbs. (C) Representative histogram showing SLAM expression on $CD4^+$ T cells cultured with anti-LFA-1α (left) or anti-LFA-3 (right) MAbs. (D) Relative inhibition of the increase in the frequency of $SLAM^{hi}$ $CD4^+$ T cells. The percent inhibition in the frequency of $SLAM^{hi}$ $CD4^+$ T cells by 10 μg/ml of anti-LFA-1α or anti-LFA-3 MAbs was arbitrarily designated 100%. The bars represent the mean ± SEM ($n = 3$).

hibitory effect of anti-LFA-3 MAb was observed at concentrations as low as 0.1 μg/ml (Fig. 5D).

To confirm whether the inhibition of HIV-1-associated SLAM upregulation by these blocking antibodies also resulted in reduced MV infectivity in $CD4^+$ T cells, HIV-1_{NL-D}-infected PBMCs cultured in the presence of blocking antibodies were infected with MVwt ($n = 2$). As expected, although the frequency of MVwt-infected $CD4^+$ T cells was increased by HIV-1 infection (from 1.30% to 4.51% for donor 1 and from 2.59% to 7.63% for donor 2), the frequency of MVwt-infected cells was reduced by anti-LFA-1α (1.21% and 5.01% for donor 1 and donor 2, respectively) and more strongly by anti-LFA-3 (1.34% and 3.63% for donor 1 and donor 2, respectively) (see Fig. S2 in the supplemental material). These data clearly indicate that SLAM upregulation and the resulting increase in MV-infected $CD4^+$ T cells are mediated by cell-to-cell contact through the interaction of costimulatory molecules that are highly expressed on HLA-DR^+ DC subsets in HIV-1-infected PBMC cultures.

DISCUSSION

The present study shows that HIV-1 infection enhanced MV infection in $CD4^+$ T cells. Interestingly, we observed that the frequencies of MVvac-infected $CD4^+$ T cells were higher than those of MVwt in both HIV-1-infected and -uninfected PBMCs. This difference may be explained by different receptor usage (4) and by differences in polymerase activity between the wild-type and vaccine strains (1) used in this study. In addition, both strains of MV inhibited HIV-1 replication (Fig. 1C), which is consistent with previous reports (7, 8, 10). Although the precise mechanism(s) underlying HIV-1 suppression by MV is not completely understood, the reduction of p24 antigen observed in the culture supernatant occurred in parallel with the elimination of HIV-1-infected cells after MV infection. It is speculated that MV infection causes apoptosis of HIV-1-infected cells directly through the expression of viral nucleoprotein and hemagglutinin proteins (2, 13, 15, 28) or through the induction of cell G_0/G_1 arrest (8), although no doubly infected $CD4^+$ T cells were detected in the culture system used in the present study. Alternatively, considering the fact that HIV-1-infected $CD4^+$ T cells are already activated, they may be hyperactivated by MV, resulting in activation-induced cell death (11).

Because MV utilizes SLAM as a receptor, it is very likely that the enhanced MV infection observed in this *ex vivo* MV and HIV-1 coinfection model was due to HIV-1-induced upregulation of SLAM. Meroni et al. showed that SLAM expression on $CD4^+$ T cells *ex vivo* is diminished during the early phase of HIV infection (16). In addition, SLAM expression on $CD4^+$ T cells was different in patients recently and chronically infected with HIV-1 (16). SLAM expression on $CD4^+$ T cells from HIV-1-infected individuals may fluctuate depending on the activation state of the immune system *in vivo*. It is important to note that most $CD4^+$ T cells within the *ex vivo* PBMC population were in the resting state and that SLAM expression was transiently downregulated soon after the initiation of culture (unpublished observation). SLAM is expressed on activated cells, and chronic hyperactivation is a characteristic feature of HIV-1 infection (11). It was assumed that $CD4^+$ T cells in the PBMC cultures were not hyperactivated and were, rather, akin to the cells within the lymphoid organs, in which a variety of antigen-presenting cells (APCs) and T cells are in contact with each other and where HIV-1 replication/expansion occurs. Therefore, it is possible that SLAM expression is upregulated in lymphoid organs during HIV-1 infection, which may enhance the infectivity of MV.

One of the aims of the present study was to examine the mechanism(s) by which HIV-1 infection enhances SLAM expression on $CD4^+$ T cells. IFN-γ upregulates SLAM expression on T cells in patients with tuberculosis (9, 23). However, neither IFN-γ nor any other soluble factors played a major role in the SLAM upregulation observed in this study. It is possible that SLAM upregulation by IFN-γ is a specific feature of certain T cells reactive to *Mycobacterium tuberculosis*. Nevertheless, the low level of SLAM upregulation induced in T cell culture may be mediated by cytokines, including IFN-γ.

In the present study, blocking experiments showed that cell-to-cell contact (presumably DCs to $CD4^+$ T cells) via LFA-1/ICAM-1 and LFA-3/CD2 interactions enhanced SLAM expression on $CD4^+$ T cells (Fig. 5). Inhibition of the LFA-3/CD2 interaction led to a more marked abrogation of SLAM expression than inhibition of the LFA-1/ICAM-1 interaction. It is noteworthy that a previous study also showed that the LFA-3/CD2 interaction was more important than the LFA-1/ICAM-1 interaction for antigen-dependent DC-T cell synapse formation (27). Therefore, CD2 costimulatory signals, in addition to TcR signals, may be involved in SLAM upregulation. Potential candidate APCs that interact with $CD4^+$ T cells to upregulate SLAM on $CD4^+$ T cells in HIV-infected PBMC cultures could be HLA-DR^+ DCs.

In conclusion, the precise mechanism(s) by which MV exacerbates the disease outcomes in HIV-1-infected individuals remains unknown. The present study, which employed a PBMC-based *ex vivo* HIV-1 and MV coinfection model, showed that increased susceptibility to MV infection involves induction of a high level of SLAM expression by HIV-1 infection via cell-to-cell contact. This is the first report showing a direct relationship between HIV-1 infection and SLAM expression. The high mortality and morbidity of measles in children coinfected with HIV-1 and MV may be due to upregulation of SLAM expression on $CD4^+$ T cells, which presumably occurs within lymphoid organs through T cell contact with DCs during HIV-1 infection. Further *in vivo* coinfection studies in a macaque model should help to clarify these outstanding issues.

ACKNOWLEDGMENTS

We thank Kahori Okano for her excellent technical assistance.

This work was supported by a grant from the Ministry of Health, Labor, and Welfare of Japan. Y.-Y. Mitsuki receives support from the Japanese Foundation for AIDS Prevention.

REFERENCES

1. **Bankamp B, Kearney SP, Liu X, Bellini WJ, Rota PA.** 2002. Activity of polymerase proteins of vaccine and wild-type measles virus strains in a minigenome replication assay. J. Virol. 76:7073–7081.
2. **Bhaskar A, Bala J, Varshney A, Yadava P.** 2011 Expression of measles virus nucleoprotein induces apoptosis and modulates diverse functional proteins in cultured mammalian cells. PLoS One 6:e18765. doi:10.1371/journal.pone.0018765.
3. **Cocks BG, et al.** 1995. A novel receptor involved in T-cell activation. Nature 376:260–263.
4. **Condack C, Grivel JC, Devaux P, Margolis L, Cattaneo R.** 2007. Measles virus vaccine attenuation: suboptimal infection of lymphatic tissue and tropism alteration. J. Infect. Dis. 196:541–549.
5. **Erlenhoefer C, et al.** 2001. CD150 (SLAM) is a receptor for measles virus but is not involved in viral contact-mediated proliferation inhibition. J. Virol. 75:4499–4505.

6. **Fujino M, et al.** 2007. Development of a new neutralization test for measles virus. J. Virol. Methods **142**:15–20.
7. **Garcia M, Yu XF, Griffin DE, Moss WJ.** 2005. In vitro suppression of human immunodeficiency virus type 1 replication by measles virus. J. Virol. **79**:9197–9205.
8. **Garcia M, Yu XF, Griffin DE, Moss WJ.** 2008. Measles virus inhibits human immunodeficiency virus type 1 reverse transcription and replication by blocking cell-cycle progression of CD4+ T lymphocytes. J. Gen. Virol. **89**:984–993.
9. **Garcia VE, et al.** 2001. Signaling lymphocytic activation molecule expression and regulation in human intracellular infection correlate with Th1 cytokine patterns. J. Immunol. **167**:5719–5724.
10. **Grivel JC, Garcia M, Moss WJ, Margolis LB.** 2005. Inhibition of HIV-1 replication in human lymphoid tissues ex vivo by measles virus. J. Infect. Dis. **192**:71–78.
11. **Haas A, Zimmermann K, Oxenius A.** 2011. Antigen-dependent and -independent mechanisms of T and B cell hyperactivation during chronic HIV-1 infection. J. Virol. **85**:12102–12113.
12. **Hashimoto K, et al.** 2002. SLAM (CD150)-independent measles virus entry as revealed by recombinant virus expressing green fluorescent protein. J. Virol. **76**:6743–6749.
13. **Iwasa T, Suga S, Qi L, Komada Y.** 2010. Apoptosis of human peripheral blood mononuclear cells by wild-type measles virus infection is induced by interaction of hemagglutinin protein and cellular receptor, SLAM via caspase-dependent pathway. Microbiol. Immunol. **54**:405–416.
14. **Kruse M, et al.** 2001. Signaling lymphocytic activation molecule is expressed on mature CD83+ dendritic cells and is up-regulated by IL-1 beta. J. Immunol. **167**:1989–1995.
15. **Laine D, et al.** 2005. Measles virus nucleoprotein induces cell-proliferation arrest and apoptosis through NTAIL-NR and NCORE-FcgammaRIIB1 interactions, respectively. J. Gen. Virol. **86**:1771–1784.
16. **Meroni L, et al.** 1999. Altered signaling lymphocytic activation molecule (SLAM) expression in HIV infection and redirection of HIV-specific responses via SLAM triggering. Clin. Immunol. **92**:276–284.
17. **Moss WJ, Cutts F, Griffin DE.** 1999. Implications of the human immunodeficiency virus epidemic for control and eradication of measles. Clin. Infect. Dis. **29**:106–112.
18. **Moss WJ, et al.** 2008. HIV type 1 infection is a risk factor for mortality in hospitalized Zambian children with measles. Clin. Infect. Dis. **46**: 523–527.
19. **Moss WJ, et al.** 2007. Immunogenicity of standard-titer measles vaccine in HIV-1-infected and uninfected Zambian children: an observational study. J. Infect. Dis. **196**:347–355.
20. **Muhlebach MD, et al.** 2011. Adherens junction protein nectin-4 is the epithelial receptor for measles virus. Nature **480**:530–533.
21. **Noyce RS, et al.** 2011. Tumor cell marker PVRL4 (nectin 4) is an epithelial cell receptor for measles virus. PLoS Pathog. 7:e1002240. doi:10.1371/journal.ppat.1002240.
22. **Ono N, et al.** 2001. Measles viruses on throat swabs from measles patients use signaling lymphocytic activation molecule (CDw150) but not CD46 as a cellular receptor. J. Virol. **75**:4399–4401.
23. **Pasquinelli V, et al.** 2004. Expression of signaling lymphocytic activation molecule-associated protein interrupts IFN-gamma production in human tuberculosis. J. Immunol. **172**:1177–1185.
24. **Permar SR, et al.** 2007. Clinical measles after measles virus challenge in simian immunodeficiency virus-infected measles virus-vaccinated rhesus monkeys.. J. Infect. Dis. **196**:1784–1793.
25. **Shen A, et al.** 2007. Novel pathway for induction of latent virus from resting $CD4^+$ T cells in the simian immunodeficiency virus/macaque model of human immunodeficiency virus type 1 latency.. J. Virol. **81**: 1660–1670.
26. **Takeda M, et al.** 2006. Generation of measles virus with a segmented RNA genome. J. Virol. **80**:4242–4248.
27. **Tsunetsugu-Yokota Y, et al.** 1997. Efficient virus transmission from dendritic cells to CD4+ T cells in response to antigen depends on close contact through adhesion molecules. Virology **239**:259–268.
28. **Vuorinen T, Peri P, Vainionpaa R.** 2003. Measles virus induces apoptosis in uninfected bystander T cells and leads to granzyme B and caspase activation in peripheral blood mononuclear cell cultures. Eur. J. Clin. Invest. **33**:434–442.
29. **Yamamoto T, et al.** 2009. Selective transmission of R5 HIV-1 over X4 HIV-1 at the dendritic cell-T cell infectious synapse is determined by the T cell activation state. PLoS Pathog. 5:e1000279. doi:10.1371/journal.ppat.1000279.

PLOS ONE

Expansion of Activated Memory CD4$^+$ T Cells Affects Infectivity of CCR5-Tropic HIV-1 in Humanized NOD/SCID/JAK3^{null} Mice

Kazutaka Terahara[1☯], Masayuki Ishige[1,2☯], Shota Ikeno[1,3], Yu-ya Mitsuki[1], Seiji Okada[2], Kazuo Kobayashi[1], Yasuko Tsunetsugu-Yokota[1]*

1 Department of Immunology, National Institute of Infectious Diseases, Tokyo, Japan, **2** Division of Hematopoiesis, Center for AIDS Research, Kumamoto University, Kumamoto, Japan, **3** Laboratory of Viral Infection II, Kitasato Institute for Life Science, Kitasato University, Tokyo, Japan

Abstract

Humanized mice reconstituted with human hematopoietic cells have been developed as an experimental animal model for human immunodeficiency virus type 1 (HIV-1) infection. Myeloablative irradiation is usually performed to augment the engraftment of donor hematopoietic stem cells (HSCs) in recipient mice; however, some mouse strains are susceptible to irradiation, making longitudinal analysis difficult. We previously attempted to construct humanized NOD/SCID/JAK3^{null} (hNOJ) mice, which were not irradiated prior to human HSC transplantation. We found that, over time, many of the reconstituted CD4$^+$ T cells expanded with an activated effector memory phenotype. Therefore, the present study used hNOJ mice that were irradiated (hNOJ (IR+)) or not (hNOJ (IR−)) prior to human HSC transplantation to examine whether the development and cellularity of the reconstituted CD4$^+$ T cells were influenced by the degree of chimerism, and whether they affected HIV-1 infectivity. Indeed, hNOJ (IR+) mice showed a greater degree of chimerism than hNOJ (IR−) mice. However, the conversion of CD4$^+$ T cells to an activated effector memory phenotype, with a high percentage of cells showing Ki-67 expression, occurred in both hNOJ (IR+) and hNOJ (IR−) mice, probably as a result of lymphopenia-induced homeostatic expansion. Furthermore, when hNOJ (IR+) and hNOJ (IR−) mice, which were selected as naïve- and memory CD4$^+$ T cell subset-rich groups, respectively, were infected with CCR5-tropic HIV-1 *in vivo*, virus replication (as assessed by the plasma viral load) was delayed; however, the titer subsequently reached a 1-log higher level in memory-rich hNOJ (IR−) mice than in naïve-rich hNOJ (IR+) mice, indicating that virus infectivity in hNOJ mice was affected by the different status of the reconstituted CD4$^+$ T cells. Therefore, the hNOJ mouse model should be used selectively, i.e., according to the specific experimental objectives, to gain an appropriate understanding of HIV-1 infection/pathogenesis.

Citation: Terahara K, Ishige M, Ikeno S, Mitsuki Y-y, Okada S, et al. (2013) Expansion of Activated Memory CD4$^+$ T Cells Affects Infectivity of CCR5-Tropic HIV-1 in Humanized NOD/SCID/JAK3^{null} Mice. PLoS ONE 8(1): e53495. doi:10.1371/journal.pone.0053495

Editor: Roberto F. Speck, University Hospital Zurich, Switzerland

Received August 3, 2012; **Accepted** November 29, 2012; **Published** January 2, 2013

Funding: This work was supported by grants from the Ministry of Education, Science, Sports and Culture of Japan (K.T.), and the Ministry of Health, Labour and Welfare of Japan (K.T. and Y.T.Y.). The funders had no role in study design, data collection and analysis, decision to publish, or preparation of the manuscript.

Competing Interests: The authors have declared that no competing interests exist.

* E-mail: yyokota@nih.go.jp

☯ These authors contributed equally to this work.

Introduction

Human immunodeficiency virus type 1 (HIV-1), the causative agent of acquired immunodeficiency syndrome (AIDS) in humans, infects CD4$^+$ T cells as well as macrophages and dendritic cells by binding to its primary receptor, CD4, and a co-receptor, usually CCR5 or CXCR4 [1,2,3]. Not only is the tropism of HIV-1 determined by its use of either CCR5 or CXCR4, but factors such as cellular activation status, differentiation and maturation status, cell type, and the histological location of the target cells also determine HIV-1 infectivity with respect to its replication, dissemination, and latency [4,5,6]. *In vivo* studies are essential if we are to better understand the dynamics of HIV-1 infection and pathogenesis, in addition to improving the trials of putative anti-HIV/AIDS drugs, gene therapy, and vaccines. Therefore, the development of suitable experimental animal models is desirable. Mice reconstituted with human hematopoietic cells, referred to as humanized mice, have recently attracted attention as experimental animal models of HIV-1 infection [7,8,9,10,11,12].

At present, bone marrow/liver/thymus (BLT) mice, which are produced by surgical implantation of human fetal thymus and liver tissue into NOD/SCID mice, followed by transplantation of autologous fetal liver CD34$^+$ hematopoietic stem cells (HSCs), seem to be an ideal humanized mouse model because they support T cell development in a human thymic environment and generate human MHC-restricted T cell responses *in vivo* [13]. However, due to the ethical issues surrounding the use of fetal organs, studies using BLT mice are limited. Therefore, Rag2^{null}IL2Rγ^{null} mice (including BRG (BALB/c-background) and B6RG (C57BL/6-background) mice), or NOD/SCID/IL2Rγ^{null} mice (including NOG (truncated IL-2Rγ chain lacking the intracytoplasmic domain) and NSG (complete absence of IL-2Rγ chain) mice) are conventionally used as recipients of transplanted human HSCs [7,9,10,12,14,15,16]. In addition, BALB/c-Rag1^{null}IL2Rγ^{null} mice [17] and NOD/SCID/JAK3^{null} (NOJ) mice [18] have

recently been developed as an alternative recipient mouse strain, thereby providing more options for the construction of humanized mice.

Various methods are used to construct humanized mice [12,14,19]. The key issue is the efficiency of HSC engraftment [19,20,21]. Myeloablative irradiation is conventionally performed to augment the engraftment of donor HSCs within the recipient bone marrow (BM) [22], although irradiation may shorten the life-span of certain strains of mice [17,18,22,23]. Hence, it is difficult to study prolonged HIV-1 infection/pathogenesis using certain strains of irradiated mice. To overcome this problem, Watanabe *et al.* proposed the use of non-irradiated humanized NOG mice, as they have a longer life-span and support HIV-1 infection for over 3 months [22]. For this reason, we attempted to construct a humanized mouse model based on NOJ mice (hNOJ mice) that were not irradiated prior to HSC transplantation. Our preliminary study showed that many of the $CD4^+$ T cells that were reconstituted in hNOJ mice expanded with an activated effector memory phenotype over time. Because non-irradiated humanized mice reconstitute human hematopoietic cells less efficiently [22], non-irradiated hNOJ mice may provide a lymphopenic environment that favors lymphopenia-driven homeostatic proliferation (HSP) of T cells. Lymphopenia-induced HSP involves both slowly and rapidly proliferating $CD4^+$ T cells: the former remain phenotypically naïve, whereas the latter convert from a naïve to a memory-like phenotype with a greater activation potential [24,25,26]. The occurrence of T cell HSP, particularly in the latter case, is supported by other conventional humanized mouse models based on the BRG [27] and NOG [28] strains. Therefore, it is postulated that both the manner and dynamics of HIV-1 infection in humanized mice may be affected by the presence of HSP and, if so, that the humanized mouse model should be used selectively according to the specific experimental objectives.

The aim of the present study was to elucidate whether HSP of $CD4^+$ T cells was influenced by the degree of chimerism, and whether it affected HIV-1 infectivity in hNOJ mice. First, we compared the dynamics of reconstituted $CD4^+$ T cell cellularity between hNOJ mice that were irradiated (hNOJ (IR+)) or not (hNOJ (IR−)) prior to human HSC transplantation, and characterized them as high and low chimerism groups, respectively. Here, we show that the conversion of $CD4^+$ T cells to an activated effector memory phenotype occurred in both hNOJ (IR+) and hNOJ (IR−) mice over time. We also challenged hNOJ (IR+) and hNOJ (IR−) mice, which were selected as naïve- and memory $CD4^+$ T cell subset-rich groups, respectively, with CCR5-tropic (R5) HIV-1. The plasma viral load was blunted during the early phase post-challenge, but subsequently reached a 1-log higher level in memory-rich hNOJ (IR−) mice than in naïve-rich hNOJ (IR+) mice. Taken together, the results of the present study provide useful information for evaluating the usefulness of hNOJ mice as a model of HIV-1 infection.

Methods

Ethics Statement

Human umbilical cord blood was obtained from the Tokyo Cord Blood Bank (Tokyo, Japan) after receiving written informed consent. Human peripheral blood was obtained from the Blood Bank of Japan Red Cross (Tokyo, Japan) or from healthy adult volunteers after receiving written informed consent. The use of human umbilical cord blood and peripheral blood was approved by the Institutional Ethical Committee of the National Institute of Infectious Diseases (Tokyo, Japan) (Permit Numbers: 127 and 122, respectively). All mice were treated in accordance with the guidelines set down by and approved by the Institutional Animal Care and Use Committee of the National Institute of Infectious Diseases (Permit Numbers: 208022, 109019, 110026, 211033, and 112040).

Mice

NOD/SCID/$JAK3^{null}$ (NOJ) mice were established as described previously [18] and maintained under specific pathogen-free conditions in the animal facility at the National Institute of Infectious Diseases.

Construction of Humanized Mice

Human HSCs were isolated from umbilical cord blood using a CD133 MicroBead Kit (Miltenyi Biotec Inc, Auburn, CA). The purity was approximately 90% as assessed by flow cytometric analysis of CD34 expression. Human HSCs ($0.5-1\times10^5$ cells) were transplanted into the livers of irradiated (1 Gy) or non-irradiated newborn mice within 2 days of birth. The number of hNOJ mice used and the ID number of the donor from which hNOJ mice were derived are listed in Table 1.

Cell Preparation

Human peripheral blood mononuclear cells (PBMCs) were separated by a Ficoll-Hypaque density gradient (Lymphosepal; IBL, Gunma, Japan). For hNOJ mice, peripheral blood, spleens and BM were collected and the red blood cells were lysed in ACK buffer (0.15 M NH_4Cl, 1 mM $KHCO_3$, and 0.1 mM EDTA-2Na; pH 7.2−7.4). In some cases, $CD4^+$ T cells from human PBMCs or hNOJ splenocytes were negatively selected using an EasySep Human $CD4^+$ T cell Enrichment Kit (StemCell Technologies, Vancouver, BC, Canada), or a combination of this kit and a StemSep Mouse/Human Chimera Enrichment Kit (StemCell Technologies), respectively. The purity was ≥95% as assessed by flow cytometry.

Flow Cytometry

Cells were stained with fluorescence-conjugated monoclonal antibodies as described previously [29]. The following antibodies were used for flow cytometry in various combinations: FITC-conjugated anti-mouse CD45 (30-F11), anti-human CD34 (581), and CD195/CCR5 (HEK/1/85a); PE-conjugated anti-human CD19 (HIB19), CD150 (A12(7D4)), CD184/CXCR4 (12G5) and IFN-γ (4S.B3); PerCP-conjugated anti-human CD3 (UCHT1), CD4 (RPA-T4), CD8a (RPA-T8), and HLA-DR (L243); PE-Cy7-conjugated anti-human CD3 (UCHT1); APC-conjugated anti-human CD8a (RPA-T8) and CD45RA (HI100); Alexa Fluor 647-conjugated anti-human CD25 (BC96); Alexa Fluor 700-conjugated anti-human CD4 (OKT4), CD27 (O323) and CD69 (FN50); Pacific Blue-conjugated anti-human CD3 (UCHT1), CD4 (RPA-T4), and CD45 (HI30) (all purchased from BioLegend, San Diego, CA). FITC-conjugated anti-human Ki-67 (B56) and PE-Cy7-conjugated anti-human CD197/CCR7 (3D12) were purchased from BD Biosciences (San Diego, CA). APC-conjugated anti-human CD14 (TÜK4) was purchased from Miltenyi Biotec Inc. Anti-human CD11a (TS1/22.1.1.13) and CD38 (OKT10) antibodies were prepared from hybridoma cells (ATCC Nos. HB202 and CRL8022, respectively) and were conjugated with Alexa Fluor 647 and Alexa Fluor 700, respectively, using Alexa Fluor succinimidyl esters (Invitrogen, Carlsbad, CA). Dead cells were stained with propidium iodide or with a LIVE/DEAD Fixable Dead Cell Stain Kit (L34957; Invitrogen) and were gated out during analysis. Intracellular staining for Ki-67 and IFN-γ was performed using a BD Cytofix/Cytoperm Fixation/Permeabiliza-

Table 1. The number of mice used in the present study.

Figure	Number of NOJ mice				Notes
	IR+		IR−		
	Total	Composition (donor #)	Total	Composition (donor #)	
Figure 1					
A	16	2 (D56), 3 (D57), 3 (D59), 1 (D62), 1 (D63), 1 (D65), 1 (D69), 1 (D74), 3 (D80)	28	3 (D47), 2 (D49), 2 (D51), 1 (D52), 2 (D56), 2 (D57), 3 (D59), 2 (D65), 3 (D67), 1 (D68), 2 (D69), 1 (D74), 4 (D80)	
B	7	3 (G65), 1 (G69), 3 (G80)	10	3 (D65), 3 (D69), 4 (D80)	
Figure 2					
A, D, E	22	1 (D56), 3 (D57), 3 (D59), 4 (D62), 5 (D63), 3 (D65), 3 (D80)	13	2 (D56), 2 (D57), 2 (D59), 3 (D65), 4 (D80)	
B, C	5	1 (D54), 2 (D60), 1 (D104), 1 (D105)	6	4 (D54), 1 (D60), 1 (D110)	
Figure 3					
A	1[a]	1 (D65)			[a]Representative of Figure 3B
B	18	3 (D57), 2 (D59), 2 (D62), 5 (D63), 3 (D65), 1 (D69), 2 (D80)	6	3 (D47), 2 (D57), 1 (D80)	
Figure 4					
A	18	[b]	6	[b]	[b]Same as in Figure 3B
B	2	2 (D114)	4	1 (D1), 2 (D3), 1 (D4)	
C	1[c]	1 (D80)			[c]Representative of 4 IR+ mice
D	2	2 (D80)	2	2 (D80)	
E	25	3 (D57), 3 (D59), 4 (D62), 5 (D63), 2 (D64), 3 (D65), 2 (D69), 3 (D80)	21	3 (D47), 2 (D57), 3 (D59), 3 (D65), 3 (D67), 1 (D68), 3 (D69), 3 (D80)	
Figure 5					
A	12	3 (D65), 1 (D90), 6 (D101), 1 (D113), 1 (D114)	8	2 (D59), 1 (D65), 1 (D74), 1 (D85), 3 (D92)	
B	6	2 (D80), 1 (D101), 2 (D113), 1 (D114)	6	3 (D80), 3 (D92)	
C	1[d]	1 (G113)			[d]Representative of Figure 5D
D	3	2 (D113), 1 (D114)	3	3 (D92)	
Figure 6					
A, B	18	[b]	6	2 (D57), 1 (D59), 2 (D69), 1 (D80)	[b]Same as in Figure 3B
C	1[e]	1 (D65)			[e]Representative of Figure 6D
D, E	3	3 (D65)	1	1 (D59)	
Figure 7					
A, B, C	7	7 (D101)	8	2 (D13), 1 (D23), 5 (D122)	
D	6[f]	6 (D101)	7[f]	2 (D13), 1 (D23), 4 (D122)	[f]Included in Figure 7A, B, C
Figure 8			3	3 (D33)	

doi:10.1371/journal.pone.0053495.t001

tion Solution (BD Biosciences) or a FIX & PERM Fixation and Permeabilization Kit (Invitrogen). Absolute cell counts in the peripheral blood of hNOJ mice were determined using Trucount tubes (BD Biosciences). Data were collected using a FACSCanto II (BD Biosciences) and analyzed using FACSDiva software (BD Biosciences) or FlowJo software (Tree Star, San Carlos, CA).

Ex vivo IFN-γ Production in $CD4^+$ T Cells Induced by PMA/ionomycin Stimulation

Purified $CD4^+$ T cells were stimulated *ex vivo* with or without 20 ng/ml phorbol 12-myristate 13-acetate (PMA; Sigma-Aldrich, St. Louis, Mo) and 1 μg/ml ionomycin (Sigma-Aldrich) in RPMI medium containing 10% heat-inactivated fetal bovine serum, 100 μg/ml penicillin, 100 μg/ml streptomycin, 2 mM L-glutamine, 5 μg/ml brefeldin A, and 2 μM monensin at 37°C for 4 h. Intracellular IFN-γ was analyzed by flow cytometry as described above. Because PMA treatment downmodulates CD4 expression [30], and to distinguish $CD4^+$ T cells from $CD8^+$ T cells (a minor contaminant in the purified $CD4^+$ T cell fraction), $CD3^+CD8^-$ T cells were denoted as $CD4^+$ T cells in this experiment.

Detection of Cytokines in the Plasma

IL-2, IL-7, and IL-15 levels in the plasma from routinely collected peripheral blood samples were measured using a Milliplex MAP Human Cytokine/Chemokine Panel (Merck Millipore Japan, Tokyo, Japan) on a MAGPIX platform (Merck Millipore Japan).

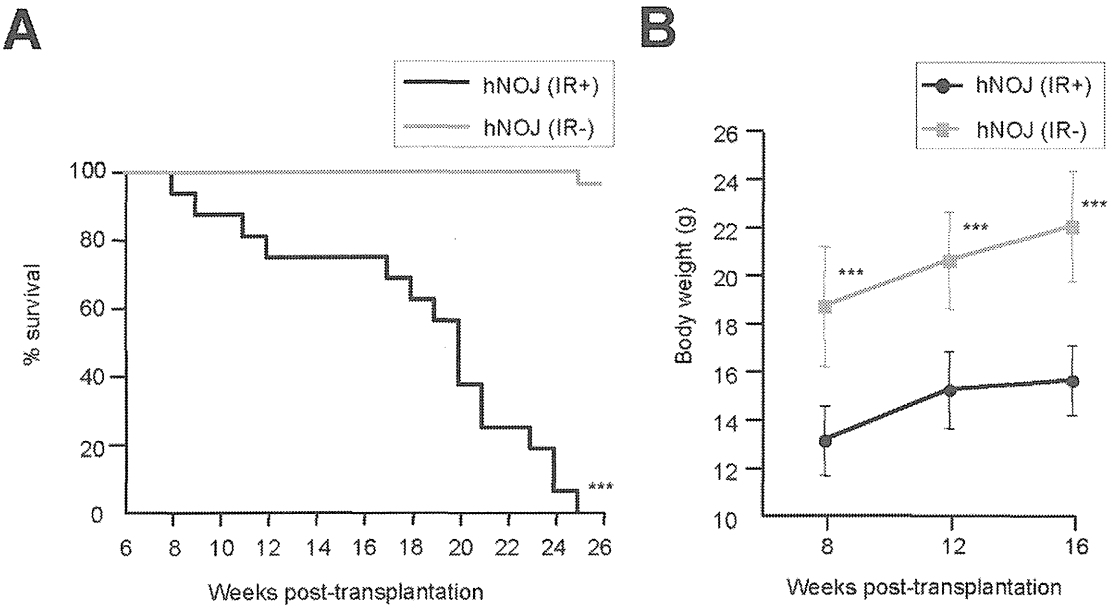

Figure 1. Influence of irradiation on the survival and growth of hNOJ mice. Newborn NOJ mice (1−2 days after birth) were irradiated (1 Gy) or not before transplantation with $CD34^+CD133^+$ HSCs isolated from human cord blood. (A) Survival curves for hNOJ (IR+) and hNOJ (IR−) mice ($n=16$ and $n=28$, respectively). Significant differences ($^{***}P<0.001$) were determined by the log-rank test. (B) Changes in the body weight of hNOJ (IR+) and hNOJ (IR−) mice ($n=7$ and $n=10$, respectively). Data are expressed as the mean ± SD. Significant differences ($^{***}P<0.001$) were determined by the unpaired t test.
doi:10.1371/journal.pone.0053495.g001

Fusion Assay

A fusion assay was performed using HIV-1 possessing β-lactamase-Vpr chimeric proteins (BlaM-Vpr) and $CD4^+$ T cells loaded with CCF2 dye, a fluorescent substrate for β-lactamase, as previously described [31,32]. In brief, R5 HIV-$1_{NL\text{-}AD8\text{-}D}$ [29] containing BlaM-Vpr (HIV-$1_{NL\text{-}AD8\text{-}D\text{-}BlaM\text{-}Vpr}$) was obtained by cotransfecting 293T cells with pNL-AD8-D plus pMM310, encoding *Escherichia coli* β-lactamase fused to the amino terminus of Vpr [33]. The purified $CD4^+$ T cells (1×10^6 cells) were infected with 200 ng of p24-measured amounts of HIV-$1_{NL\text{-}AD8\text{-}D\text{-}BlaM\text{-}Vpr}$ by spinoculation at $1200\times g$ for 2 h at 25°C as previously described [34]. After spinoculation, cells were washed and then incubated in RPMI containing 10% heat-inactivated fetal bovine serum for 2 h at 37°C to induce viral fusion. After fusion, cells were washed and loaded with CCF2-AM for 1 h at RT using a GeneBLAzer *In Vivo* Detection Kit (Invitrogen). The dye-loaded cells were incubated overnight at RT and subjected to flow cytometry. Cells permissive for HIV-1 fusion were detected at a fluorescence emission spectrum of 447 nm after excitation with a 405-nm violet laser in a FACSCanto II.

In vivo HIV-1 Infection of hNOJ Mice

hNOJ mice were challenged intravenously with 200 ng of p24-measured amounts of R5 HIV-$1_{NL\text{-}AD8\text{-}D}$, which express DsRed [29]. Peripheral blood was harvested from the HIV-1-challenged hNOJ mice on a weekly basis. All animal experiments with highly pathogenic viruses were conducted in a biosafety level 3 containment facility.

Detection of Plasma Viral RNA by Quantitative Real-time RT-PCR

Viral RNA was extracted from the plasma and purified using a QIAamp Viral RNA Mini Kit (Qiagen, Valencia, CA). The RNA was subjected to quantitative real-time RT-PCR using a SuperScript III Platinum One-Step Quantitative RT-PCR System (Invitrogen) with the following set of HIV-1 gag primers and probe [35]: forward primer, HIVgag638 (+) (5′-CTCTCGACGCAGGACTCGGCTTGCT-3′); reverse primer, HIVgag803 (−) (5′-GCTCTCGCACCCATCTCTCTCCTTC-TAGCC-3′); and HIV-1 gag probe, TaqMan 720R748 (FAM-5′-GCAAGAGGCGAGRGGCGGCGACTGGTGAG-3′-BHQ-1). PCR was performed using an Mx3000P PCR system (Stratagene, La Jolla, CA). The detection limit was set at 5000 copies/ml plasma using samples obtained from HIV-$1_{NL\text{-}AD8\text{-}D}$-challenged NOJ mice that were not transplanted with HSCs.

Statistical Analysis

The significance of the data was evaluated using an unpaired t test, a paired t test, the Mann-Whitney U test, the Wilcoxon signed rank test, Spearman's rank correlation coefficient, or Tukey's or Bonferroni multiple comparison tests based on the normality and variance of the data compared, or the Log-rank test (see individual Figure Legends). Prism ver.4 software (GraphPad Software, Inc., San Diego, CA) was used for all analyses. $P<0.05$ was considered statistically significant.

Results

Influence of Irradiation on the Survival and Growth of hNOJ Mice

We initially examined how the irradiation of recipient mice influences their survival and growth. Because infant mice were sometimes cannibalized and abandoned by their mothers, and the death of an infant could not always be attributed to irradiation, we started monitoring weaned mice from 6 wk post-transplantation. There was a significant difference between the survival curves of irradiated hNOJ (hNOJ (IR+)) and non-irradiated hNOJ (hNOJ (IR−)) mice ($n=16$ and $n=28$, respectively, $P<0.001$) (Figure 1A). At 16 wk post-transplantation, the survival rate of hNOJ (IR+)

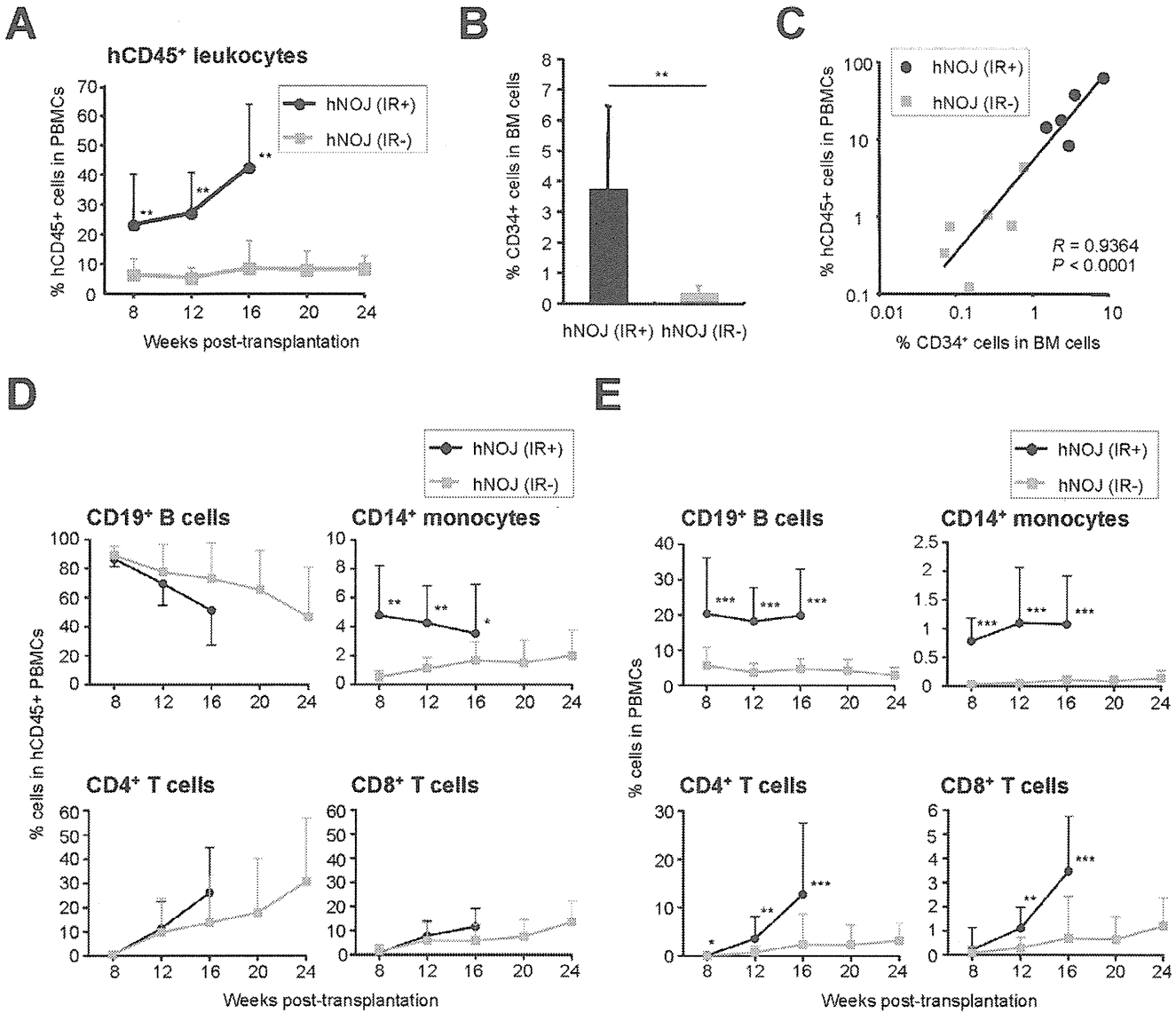

Figure 2. Development of human hematopoietic cells in hNOJ mice. (A) Changes in the percentage of human CD45$^+$ (hCD45$^+$) cells within the PBMC population from hNOJ (IR+) and hNOJ (IR−) mice ($n=22$ and $n=13$, respectively). Data are expressed as the mean ± SD. Significant differences ($^{**}P<0.01$) were determined by the Mann-Whitney U test. (B) Percentage of human CD34$^+$ cells within the BM cells isolated from hNOJ (IR+) and hNOJ (IR−) mice ($n=5$ and 6, respectively) at 8 wk post-transplantation. Data are expressed as the mean ± SD. Significant differences ($^{**}P<0.01$) were determined by the Mann-Whitney U test. (C) Association between the percentage of hCD45$^+$ cells within the PBMC population and that of CD34$^+$ cells within the BM cells of hNOJ (IR+) and hNOJ (IR−) mice at 8 wk post-transplantation (11 plots from five hNOJ (IR+) and six hNOJ (IR−) mice). Spearman's rank correlation coefficient was used for statistical analysis. (D, E) Changes in the percentage of human CD19$^+$ B cells, CD14$^+$ monocytes, CD4$^+$ T cells (CD3$^+$CD4$^+$CD8$^-$ cells), and CD8$^+$ T cells (CD3$^+$CD4$^-$CD8$^+$ cells) within the peripheral blood hCD45$^+$ cell population (D) or total PBMC populstion (E) from hNOJ (IR+) and hNOJ (IR−) mice ($n=22$ and $n=13$, respectively). Data are expressed as the mean ± SD. Significant differences ($^*P<0.05$, $^{**}P<0.01$, $^{***}P<0.001$) were determined by the Mann-Whitney U test.
doi:10.1371/journal.pone.0053495.g002

mice dramatically declined (median survival: 20.0 wk) and none survived beyond 25 wk post-transplantation (Figure 1A). However, obvious signs and symptoms of illness, such as wasting, weakness, diarrhea, hunchback posture, and alopecia, were not observed during their lifetime; although the growth of hNOJ (IR+) mice ($n=7$) was significantly stunted compared with that of hNOJ (IR−) mice ($n=10$) (Figure 1B). Although the life-span of the hNOJ (IR+) mice used in the present study was shorter than that reported previously [18], probably because of the environmental conditions in our animal facility, these results demonstrated that irradiation apparently induces high mortality and low growth in hNOJ mice. Therefore, in the present study, the averaged data obtained from hNOJ (IR+) mice surviving up until 16 wk post-transplantation are reported for all the following experiments.

Development of Human Hematopoietic Cells in hNOJ Mice

Reconstitution of human hematopoietic cells (i.e., chimerism) in hNOJ mice was investigated by flow cytometry using peripheral blood samples collected routinely (every 4 wk) after 8 wk post-transplantation. hNOJ (IR+) mice ($n=22$) showed higher chimerism (according to the percentage of human CD45$^+$ (hCD45$^+$)

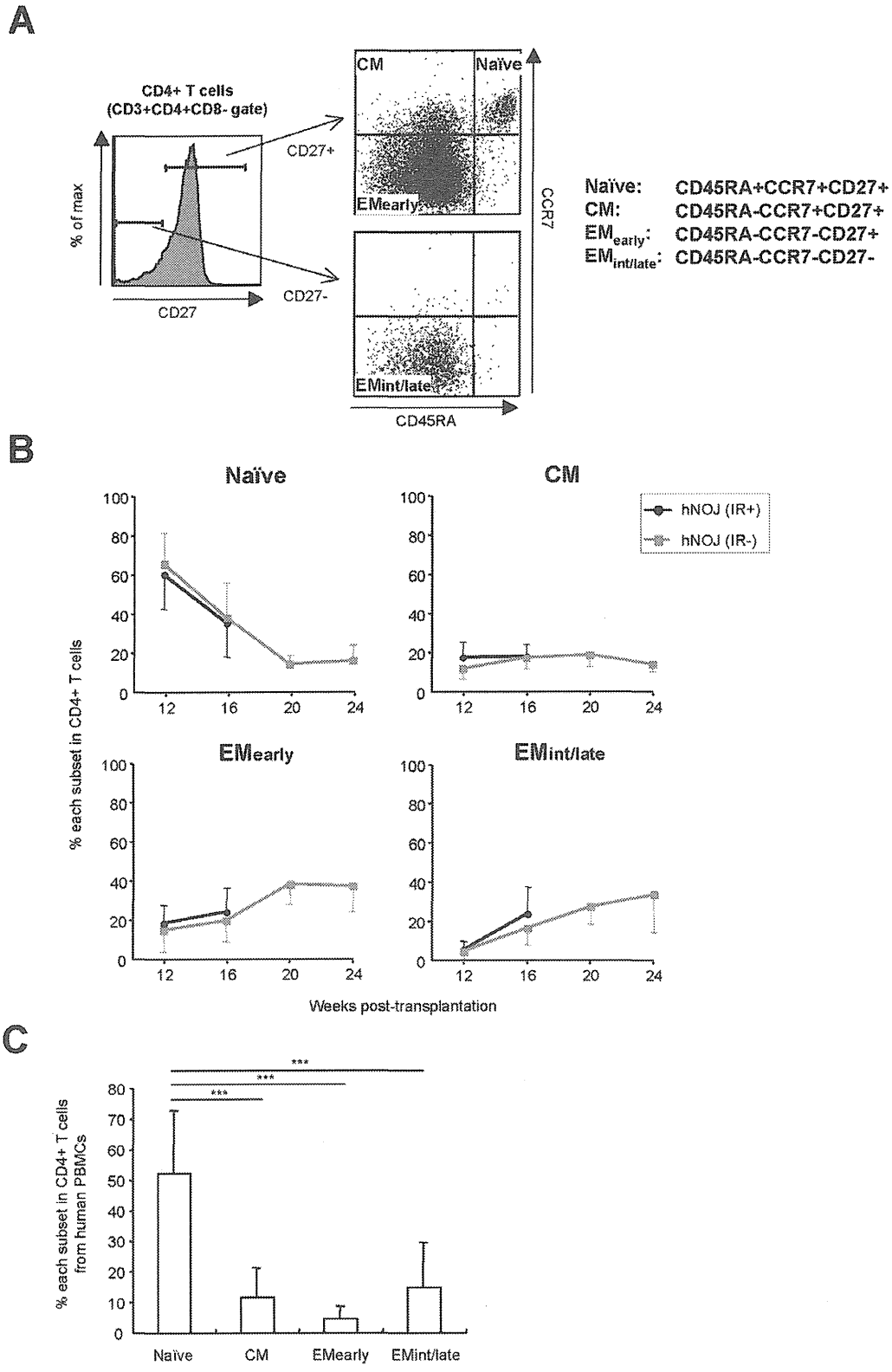

Figure 3. Differentiation of CD4$^+$ T Cells in hNOJ mice. (A) Naïve, CM, EM_{early}, and $EM_{int/late}$ subsets of CD4$^+$ T cells (gated on CD3$^+$CD4$^+$CD8$^-$) were defined as CD45RA$^+$CCR7$^+$CD27$^+$, CD45RA$^-$CCR7$^+$CD27$^+$, CD45RA$^-$CCR7$^-$CD27$^+$, and CD45RA$^-$CCR7$^-$CD27$^-$, respectively, by flow cytometry. (B) Changes in the percentage of naïve, CM, EM_{early}, and $EM_{int/late}$ subsets within the peripheral blood CD4$^+$ T cell populations isolated from hNOJ (IR+) and hNOJ (IR−) mice ($n = 18$ and $n = 6$, respectively). Data are expressed as the mean ± SD. (C) Percentage of CM, EM_{early}, and $EM_{int/late}$ subsets within human peripheral blood CD4$^+$ T cells. Data are expressed as the mean ± SD ($n = 10$). Significant differences ($^{***}P<0.001$) were determined by Tukey's multiple comparison test.
doi:10.1371/journal.pone.0053495.g003

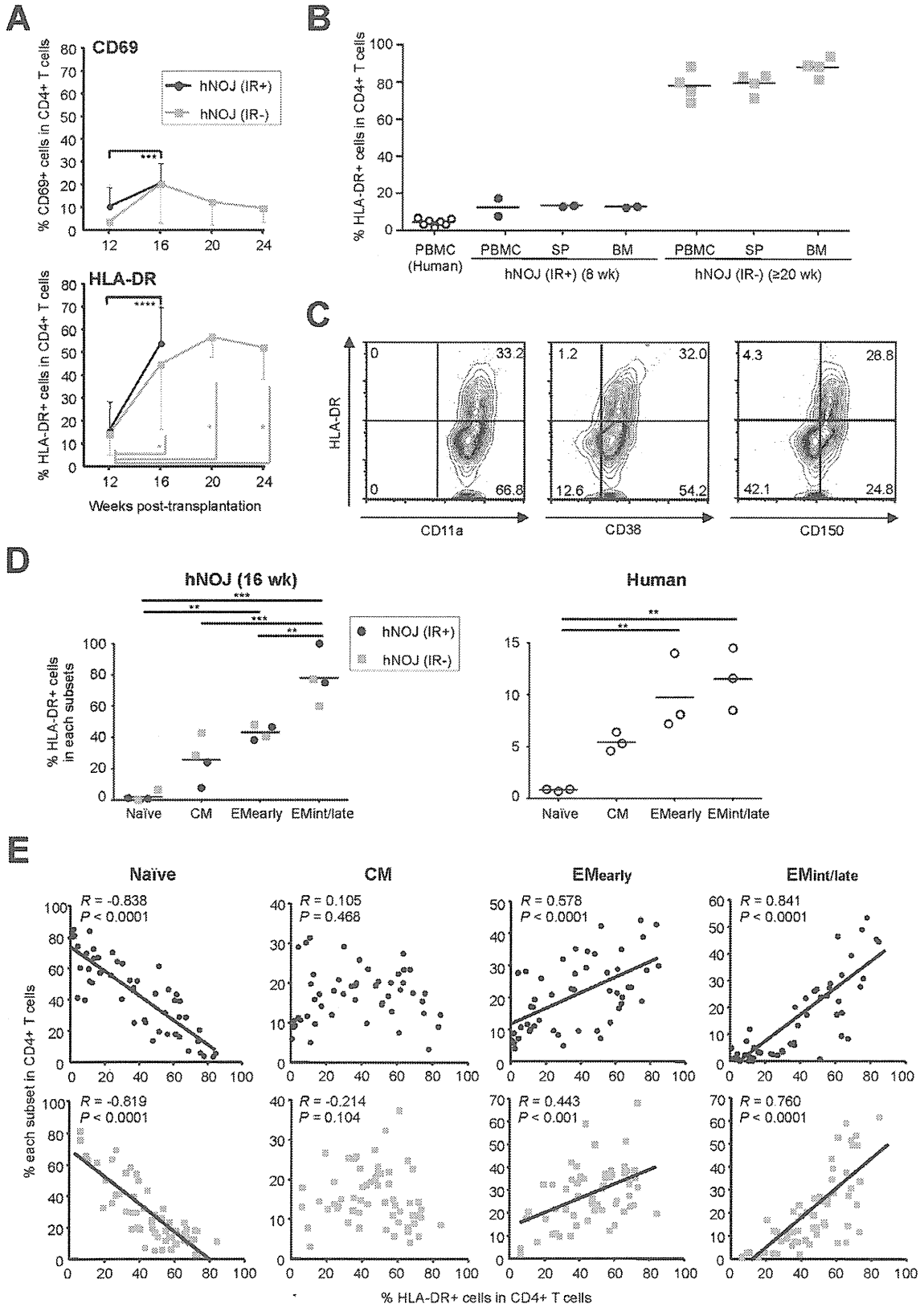

Figure 4. Activation status of CD4$^+$ T Cells in hNOJ mice. (A) Changes in the percentage of CD69$^+$ (upper) and HLA-DR$^+$ (lower) cells within the peripheral blood CD4$^+$ T cells isolated from hNOJ (IR+) and hNOJ (IR−) mice ($n = 18$ and $n = 6$, respectively). Data are expressed as the mean ± SD. Significant differences ($^*P<0.05$, $^{****}P<0.0001$) were determined using the Wilcoxon signed rank test or a paired t test. (B) Percentage of HLA-DR$^+$ cells within the CD4$^+$ T cell populations isolated from PBMCs, spleens (SP), and BM from hNOJ (IR+) mice at 8 wk post-transplantation ($n = 2$) and hNOJ (IR−) mice at ≥20 wk post-transplantation ($n = 4$), and from human PBMCs ($n = 7$). Data are plotted individually. The black line represents the mean.

(C) Expression of HLA-DR and other activation markers (CD11a, CD38, and CD150) by peripheral blood $CD4^+$ T cells. Representative flow cytometry profiles are shown from one of four hNOJ (IR+) mice at 16 wk post-transplantation. (D) Percentage of $HLA\text{-}DR^+$ cells in the naïve, CM, EM_{early}, and $EM_{int/late}$ subsets of peripheral blood $CD4^+$ T cells isolated from hNOJ mice at 16 wk post-transplantation ($n=4$; two hNOJ (IR+) and two hNOJ (IR−) mice) and from humans ($n=3$). Data are expressed as the mean ± SD. Significant differences ($^{**}P<0.01$, $^{***}P<0.001$) were determined by Tukey's multiple comparison test. (E) Association between the percentage of each $CD4^+$ T cell subset and that of $HLA\text{-}DR^+$ cells in the peripheral blood $CD4^+$ T cell population. Data were obtained from peripheral blood samples routinely collected from hNOJ (IR+) and hNOJ (IR−) mice within 28 wk post-transplantation (50 data points obtained from 25 mice (upper panels) and 59 data points obtained from 21 mice (lower panels), respectively). Spearman's rank correlation coefficient was used for statistical analysis.
doi:10.1371/journal.pone.0053495.g004

leukocytes within the total PBMC population) than hNOJ (IR−) mice ($n=13$) during the course of the experiment (Figure 2A).

Furthermore, we examined the effects of irradiation on the engraftment of HSCs in the BM of hNOJ mice in which $hCD45^+$ leucocytes were observed. hNOJ (IR+) mice showed a significantly higher percentage of $CD34^+$ cells within the total BM cell population (an average of 3.7%; $n=5$) than hNOJ (IR−) mice (an average of 0.3%; $n=6$) at 8 wk post-transplantation (Figure 2B). The percentage of $CD34^+$ cells within the total BM cell population was positively correlated with the percentage of $hCD45^+$ leukocytes within the total PBMC population at 8 wk post-transplantation ($R=0.9364$, $P<0.001$, $n=11$ [five hNOJ (IR+) and six hNOJ (IR−) mice]; Figure 2C). These results indicate that irradiation augments the chimerism of human hematopoietic cells due to the enhanced engraftment of HSCs in the BM of hNOJ mice.

Next, we investigated the development of hematopoietic cell subpopulations in hNOJ (IR+) and hNOJ (IR−) mice ($n=22$ and $n=13$, respectively). The reconstituted $hCD45^+$ leukocytes within the total PBMC populations from hNOJ (IR+) and hNOJ (IR−) mice comprised $CD19^+$ B cells, $CD14^+$ monocytes, and $CD3^+$ T cells (including $CD4^+$ and $CD8^+$ T cells); however, the development of each subpopulation was different (Figure 2D). $CD19^+$ B cells developed early in both hNOJ (IR+) and hNOJ (IR−) mice, as observed at 8 wk post-transplantation, before gradually declining over time (Figure 2D, left upper panel). $CD14^+$ monocytes also developed during the early phase post-transplantation in hNOJ (IR+) mice, but were rare in hNOJ (IR−) mice. In general, the percentage of all the subpopulations was significantly lower in hNOJ (IR−) mice than in hNOJ (IR+) mice up until 16 wk post-transplantation, although the percentage of $CD14^+$ monocytes in hNOJ (IR−) mice gradually increased with time (Fig. 2D, right upper panel). In apparent contrast to the earlier development of $CD19^+$ B cells, the development of $CD3^+$ T cells was delayed; they were clearly apparent at around 12 wk post-transplantation in both hNOJ (IR+) and hNOJ (IR−) mice (Figure 2D, left and right lower panels), consistent with previous reports of other conventional humanized mouse models [16,20,36,37]. The percentage of $CD3^+$ T cells reflected that of $CD4^+$ T cells; the level of $CD4^+$ T cells was higher than that of $CD8^+$ T cells, and their developmental level tended to be higher in hNOJ (IR+) mice than in hNOJ (IR−) mice, although no statistically significant differences were observed between hNOJ (IR+) and hNOJ (IR−) mice (Figure 2D, lower left and right panels). However, both the $CD4^+$ and $CD8^+$ T cell percentages within the total PBMC population in hNOJ (IR+) mice were significantly higher than those in hNOJ (IR−) mice at almost time-points up until 16 wk post-transplantation (Figure 2E, lower left and right panels). It is noteworthy that reconstitution of $CD4^+$ T cells was detected in more hNOJ (IR+) mice (18 of 22 mice) than hNOJ (IR−) mice (4 of 13 mice) at 8 wk post-transplantation, although the averaged percentages were slightly lower ($0.12\pm0.33\%$ and $0.02\pm0.03\%$ $CD4^+$ T cells, respectively, within the total PBMC population). The percentages of other human hematopoietic cells within the total PBMC population, such as $CD19^+$ B cells, $CD14^+$ monocytes and $CD8^+$ T cells, were also higher in hNOJ (IR+) mice than in hNOJ (IR−) mice at all time-points up to 16 wk post-transplantation (Figure 2E). Taken together, these results indicate that irradiation contributes to the greater reconstitution of human hematopoietic cells in these humanized mice.

Differentiation of $CD4^+$ T Cells in hNOJ Mice

A reliable differentiation pathway for human $CD4^+$ T cells has been proposed: an antigen-experienced naïve subset differentiates into a central memory (CM) subset, followed by differentiation into an effector memory (EM) subset, before finally differentiating into a terminal effector subset [38,39]. To investigate the differentiation stage of $CD4^+$ T cells reconstituted in hNOJ mice, we used hNOJ (IR+) and hNOJ (IR−) mice in which $CD4^+$ T cells had developed by 12 wk post-transplantation.

As shown in Figure 3A, we divided $CD4^+$ T cells into four subsets based on their expression of cell surface antigens as previously reported: naïve ($CD45RA^+CCR7^+CD27^+$), CM ($CD45RA^-CCR7^+CD27^+$), EM_{early} ($CD45RA^-CCR7^-CD27^+$) and $EM_{int/late}$ ($CD45RA^-CCR7^-CD27^-$) [38,40,41]. Flow cytometric analysis using PBMCs routinely collected from hNOJ (IR+) and hNOJ (IR−) mice ($n=18$ and $n=6$, respectively) demonstrated that the percentage of each $CD4^+$ T cell subset showed similar changes in hNOJ (IR+) and hNOJ (IR−) mice by 16 wk post-transplantation (Figure 3B). The naïve subset was dominant at 12 wk post-transplantation; however, the percentage decreased markedly, reaching a steady level of approximately 20% at 20 wk post-transplantation in hNOJ (IR−) mice. In sharp contrast with the changes over time observed for the naïve subset, the percentages of the EM_{early} and $EM_{int/late}$ subsets in hNOJ (IR−) mice gradually increased over time. The percentage of the CM subset in hNOJ (IR−) mice remained unchanged at 10−20% throughout the course of the experiment. The percentage of each subset in the hNOJ mice during the early phase (12 wk) post-transplantation was almost identical to that in human PBMCs, in which the naïve subset was also dominant (approximately 50%, $n=10$) (Figure 3C).

Activation Status of $CD4^+$ T Cells in hNOJ Mice

The activation status of the reconstituted $CD4^+$ T cells was assessed by flow cytometric analysis of PBMCs isolated from hNOJ (IR+) and hNOJ (IR−) mice ($n=18$ and $n=6$, respectively), based on their expression of early and late activation markers (CD69 and HLA-DR, respectively). We found that the percentage of $CD69^+CD4^+$ T cells increased in hNOJ (IR+) mice at 16 wk post-transplantation compared with that observed at 12 wk post-transplantation ($P=0.0007$). In hNOJ (IR−) mice, the percentage of $CD69^+CD4^+$ T cells appeared to show a transient increase at 16 wk post-transplantation; however, no significant differences were observed between 16 wk post-transplantation and the other time-points (Figure 4A, upper panel). By contrast, the percentage of $HLA\text{-}DR^+CD4^+$ T cells increased in both hNOJ (IR+) and hNOJ (IR−) mice at 16 wk post-transplantation compared with